A Dissertation Report

on

LOW COST AND HIGH EFFICIENCY SILICON NANOWIRE BASED SOLAR CELL

Submitted in Partial Fulfillment of the Requirement for the Award of the Degree

of

MASTER OF TECHNOLOGY

In

SOLID STATE ELECTRONIC MATERIALS

SUBMITTED BY

RAVI KUMAR VERMA

Enrollment no. 16550009

UNDER THE SUPERVISION OF

Dr. ARUP SAMANTA

(Assistant Professor)

DEPARTMENT OF PHYSICS

INDIAN INSTITUTE OF TECHNOLOGY ROORKEE

ROORKEE – 247667

May 2018

CANDIDATE'S DECLARATION

I hereby declare that the work, which is being presented in this project report entitled **"Low Cost and High Efficiency Silicon Nanowire Based Solar Cell "** submitted in partial fulfillment of the requirement for the award of degree of **Master of Technology** in **Solid State Electronic Materials**, submitted in the **Department of Physics**, **Indian Institute of Technology Roorkee**, is an authentic record of my own work carried out under the guidance of **Dr. Arup Samanta**, **(**Assistant Professor) , Department of physics, Indian Institute of Technology Roorkee.

Date:
Place: Roorkee

RAVI KUMAR VERMA
Enrollment no.-16550009
M.Tech (IInd Year)
Department of Physics
Indian Institute Technology Roorkee

CERTIFICATE

This is to certify that the above declaration made by the candidate is correct to the best of my knowledge and belief.

Dr. Arup Samanta
Assistant Professor
Department of Physics
Indian Institute of Technology Roorkee

ACKNOWLEDGEMENT

I would like to express my heartfelt gratitude to the following people who have rendered their support during my course of work. Without their assistance, this project will not have been possible. They are:

My supervisor **Dr. Arup Samanta (**Assistant Professor), Department of Physics, Indian Institute of Technology Roorkee, who is always willing to solve my queries despite their busy schedule. Their invaluable advice and experience have certainly motivated me to gain a deeper insight into the fabrication and simulation world.

I would like express my gratitude for **HOD**, Center of Nanotechnology who provided me space in High Temperature Lab. **Dr. P. Gopinath** (Assistant Professor), Department of Biotechnology, **Prof. Anirban Mitra** (Associate Professor) and **Dr. Yogesh Kumar Sharma**, Department of Physics, Indian Institute of Technology Roorkee, who allowed me use their Lab equipment whenever I needed during the course of my project work.

My **parents**; their blessing, motivation and inspiration have always provide me a high mental support and contributed in all possible way, in completion of this project work.

I am also grateful to my **friends** who are actively involved in providing me vital support and encouragement whenever I needed.

Ravi Kumar Verma

Abstract

Recently nanomaterials like Nanowire (NW), nanoparticle and quantum dot have shown to have enormous characteristics like lager surface to volume ration, quantum confinement effect that can be exploited by using them as an active element in the solar cells. NW structured solar cells have shown promising potential for integrated power source for Nano electronics systems such as driving element for nanowire sensors, logic gates

This thesis shows the description and exploration of unique solar cell design concept namely the radial p-n junction, Nano/micro wire array solar cell which reduces the production cost by ten times. Such design potentially enable a separate optimization of the design requirements for the light absorption and carrier extraction, which are two main necessary condition for efficient energy conversion in photovoltaic device.

The main idea of getting higher efficiency arises due to the orthogonalized charge separation i.e. charge carrier created due to the incident light get separated normal to the incident light which can be easily collected and allow to use low grade silicon without compromising with the efficiency.

SiNWs for the solar cell can be grown with top down or bottom up method, but many method uses very sophisticated instrument to grow SiNWs, though the metal assisted chemical etching can be used to grow the controlled length SiNWs at room temperature without using sophisticated instrument but still diameter controlling is difficult task. So, in thesis we have shown a new method to grow controlled length and diameter SiNWs using chemical etching process. Also we have simulated current transportation equation for the p-n radial junction, which show that by optimizing the length and diameter of SiNWs appreciable efficiency can be obtain at various defect density, which shows that low grade material can be used SiNWs based solar cell.

Contents

Candidate's Declaration i

Certificate i

Acknowledgement ii

Abstract iii

List of Figures vi-vii

List of Tables viii

1 Introduction 1-7

1.1 Energy, Climate change and Photovoltaic 1

1.2 Production of Silicon wafer for Solar Cell 3

1.3 Solar Illumination 4

1.4 The p-n Junction under Illumination 6

2 Literature Review 8-13

2.1 Current Photovoltaic Technology 8

2.2 Advantages of Nanowire Based Solar Cells 9

2.2.1 Orthogonalize Light Absorption and Carrier Transport 9

2.2.2 Light Scattering Effect 11

2.2.3 Light Trapping Effect 11

2.2.4 High Surface Area 12

2.2.5 Wider Range of Materials/Heterostructures 12

2.2.6 High Built-in Electric field 13

2.3. The Nano/ Micro wire Array Solar Cell 13

3 Physics of Solar Cell Device and Radial p-n Junction 14-23

3.1 Introduction 14

3.2 Salient Features 14

3.3 Recombination Losses 18
3.3.1 Shockley Read Hall Recombination 18
3.3.2 Band to Band Recombination 18
3.3.3 Auger Recombination 19
3.3.4 Surface Recombination 19
3.4 Effect of Doping on Radial Junction 19

4 MATLAB Simulation of the Radial p-n Junction Solar Cell 24-39
4.1 Transportation Equation in the Radial Geometry 24
4.1.1 Quasineutral Regions 26
4.1.2 Depletion Regions 27
4.2 Equation Solution 28
4.3 MATLAB Results 30
4.4 Discussion 38

5 Methodology and the Experimental Result 40-55
5.1 Methodology 40
5.1.1 Preparation of Controlled Size Nanoparticle 41
5.1.2 Self-assembled layer of Nanoparticle 43
5.1.3 Preparation of Nanowire by chemical Etching method 48
5.2 Ellipsometric Data 53

6 Conclusion and Future Work 56

A MATLAB Simulation Code 58-70
A.1 Radial p-n Junction Simulation 58
A.1.1 depletionregion.m 68
A.1.2 depletion.m 69
A.2 Simulation code for the Nano Particle Diameter 70

Bibliography 71-74

List of Figures

1.1	The different solar spectra	4
1.2	Source of solar radiation attenuation	5
1.3	Schematic of air mass.	5
1.4	Band diagram of p-n junction.	6
1.5	*J-V* characteristics of the p-n junction in the dark and under illuminated condition	7
2.1	schematic of traditional planar solar cell device	10
2.2	Schematic of vertical multi-junction solar cell device	10
2.3	Schematic of NW array solar cell with light scattering effect	11
2.4	Schematics of coaxial NW with light trapping effect	12
2.5	Schematic of radial junction array	13
3.1	Schematic of different kind of recombination in a typical solar cell.	19
3.2	Cross cestion of core/shell nanowire , profile of potentioal across the junction and energy band diagram respectively	21
3.3	Effect of doping concentration on core radius	23
4.1	Generalize band structure for p-n heterojunction structure	24
4.2	Schematic of single wire from the radial p-n junction cell and corresponding energy band diagram	25
4.3	A conventional planar solar cell and its band diagram	25
4.4	MATLAB simulated graph for $Na=N_d = 10^{14}$ cm^{-3} (a) V_{oc}, (b) J_{sc} (c) FF (d) Efficiency	31
4.5	MATLAB simulated graph for $N_a=10^{14}$ cm^{-3} and $N_d=10^{15}$ cm^{-3} (a)V_{oc}, (b) J_{sc} (c) FF (d) Efficiency	32
4.6	MATLAB simulated graph Efficiency for $N_a=10^{14}$ cm^{-3} and $N_d=10^{16}$ cm^{-3} (a)V_{oc}, (b) J_{sc} (c) FF (d)	33
4.7	MATLAB simulated graph for $N_a=10^{14}$ cm^{-3} and $N_d=10^{17}$ cm^{-3} (a)V_{oc}, (b) J_{sc} (c) FF (d) Efficiency	34
4.8	MATLAB Simulated graph for $Na=N_d = 10^{15}$ cm^{-3} (a)V_{oc}, (b) J_{sc} (c) FF (d) Efficiency	35

4.9	MATLAB simulated graph for $Na=N_d = 10^{16}\ cm^{-3}$ (a)V_{oc}, (b) J_{sc} (c) FF (d) Efficiency	36
4.10	MATLAB simulated graph for $Na=N_d = 10^{17}\ cm^{-3}$ (a)V_{oc}, (b) J_{sc} (c) FF (d) Efficiency	37
5.1	Schematic illustration for fabricating Silicon nanowire	40
5.2	Variation in diameter of nanoparticle at constant TEOS 0.17M	42
5.3	Variation in diameter of nanoparticle at constant TEOS 0.3M	43
5.4	300 nm self-assembled dispersed monolayer	44
5.5	300 nm self-assembled dispersed monolayer	45
5.6a	FESEM at the bottom of sample	46
5.6b	FESEM at the top of the sample	46
5.7a	SAM layer at low resolution	46
5.7b	SAM layer at high resolution	47
5.8	Scheme of the dip coating mechanism, where V_w-substrate withdrawal rate, V_c-monolayer growth rate, J_e- evaporation flux of solvent,J_w, J_p- entering fluxes of particle and solvent respectively	48
5.9a	Transferred pattern after nano particle removal at low resolution	49
5.9b	Transferred pattern after nano particle removal at high resolution	49
5.10a	FESEM image SiNW at 45^o angle obtain by 300nm nano particle	50
5.10b	FESEM image SiNW at 45^o angle obtain by 300nm nano particle	51
5.11a	FESEM image SiNW at 45^o angle obtain by 500nm nano particle	51
5.11b	Vertical FESEM image SiNW obtain by 500nm nano particle	52
5.12	Reflectance of bare cleaned silicon wafer	53
5.13	Reflectance of SiNW prepared with 300nm nano particle	54
5.14	Reflectance of SiNW prepared with 500nm nano particle	54

List of Tables

3.1 Comparison of the basic feature of the planer and radial geometry 17

Chapter 1

Introduction

1.1 Energy, Climate change and Photovoltaics

As the economics shows, the inverse relation between the price of a goods and availability of goods, it is clearly visible in present scenario if we talk about energy. We, the human being are totally dependent on the energy for our day to day life. Today worldwide demand of energy is increasing exponentially and the conventional energy resources such as fossil fuels, will be exhausted soon. Therefore, to meet this demand, we must find the alternative energy resources for long term goal which is also affordable for everyone. The solar cell places itself as the major candidate for obtaining energy from the sun, which convert the sunlight directly to electricity.

Another major reason for the necessity of a change towards regenerative energy sources is found in the global warming caused by air pollution on account of the carbon dioxide emission using fossil fuels. One alternative would be to substitute fossil energy by nuclear power, but the disposal and handling of the radioactive material is a problematic and involves much danger, unsolved issue until now. One of the most viable ways to solve the foreseeable world's energy crisis is to utilize the power of the sun. The energy we are getting from the sun is huge; actually 1 hour of solar radiation on earth is equivalent to the total world energy consumption in 1 year [1]. To utilize this energy direct conversion of solar radiation into electricity by solar cells has been examined and developed for several decades.

Silicon is most popular material choice for terrestrial solar cells. This is for several reasons. Firstly, silicon's bandgap almost ideally match to the solar spectrum [2]. Secondly, silicon is most abundant and cheap material on earth [3]. Thirdly, by using silicon, photovoltaic industry can utilize the wealth of knowledge that microelectronics industry has acquired over several decades of experience. Nowadays, about 85% of the worldwide solar cell production is based on silicon [4]. However, the market for photovoltaic applications being one of the fastest growing at present time, In order to reach this goal, scientific teams in companies and

academia are investigating ways to improve the efficiency of the cells and at the same time also trying to reduce the cost of solar cell.

At present, material and production costs of the existing inorganic semiconductor-based (i.e. silicon based) technology are still too high for a widespread substitution of fossil energy by energy production through solar cell. Therefore, a widespread attention is currently focused on new types of solar cell structure and materials, such as thin film, polymer, dye sensitized and NW based solar cell. Among them, NW based solar cells are seriously considered as potential candidates for the next generation of solar cells. Although till now the efficiency of such solar cells cell could not stand yet in comparison with the ones obtained with planar junction semiconductor solar cells [5][6], but cost factor should be kept in mind. NW based solar cells could potentially be produced in a much more cost effective way. The price for the material is quite low, and the production steps are very simple and considerably cheaper than planer semiconductor solar cells.

NW structured solar cells have shown promising potential for integrated power source for nanoelectronics systems such as driving element for nanowire sensors, logic gates[6] etc. The nanoparticles/nanowires have been used to improve the charge collection efficiency in polymer blend[6] and dye sensitized[6] solar cells. Further recent theoretical studies have indicated that solar cell having junction in radial direction has better solar cell performance characteristics than its planar counterpart[7]. This is because of orthogonalization of light and charge carrier transport. Which means that even with the low quality material radial junction based solar cell gives higher conversion efficiency than planar counterpart. Similarly Bozhi Tian et al. has physically fabricated lateral PIN-NW solar cell in self-powered circuits and reported the efficiency of around 3.4 percent [7].

Different groups[8],[9] have also fabricated vertical NW solar cell using bottom up approach but the conversion efficiency reported in these studies is quite low. In a recent study by W.F. Liu et al. reported strong enhancement of light absorption in single lateral silicon coaxial NW core (silicon)/shell (dielectric) type structure[10]. This enhancement of light trapping provides another dimension for designing of lateral NW based solar cell.

Professionals in the solar cell community have been trying to reduce the cost of the solar cell by using some innovative ideas to fabricate NW solar cells like[11],[12] has used VLS method to grow NW solar cells and[13] has grown NW solar cells using silica beads synthesis. But very few studies have been done on studying the parameters that affect and guide the performance of solar cells. For full utilization of solar cell potential we need to understand and optimize the parameters that affect and guide its performance

This thesis shows the description and exploration of unique solar cell design concept namely the radial p-n junction, Nano/micro wire array solar cell which reduces the production cost by ten times. Such design potentially enable a separate optimization of the design requirements for the light absorption and carrier extraction, which are two main necessary condition for efficient energy conversion in photovoltaic device. We will begin this chapter by exploring the motivation for photovoltaics in general and for this design concept in particular, and proceed in later chapters to a detailed theoretical and experimental exploration of the proposed device design.

1.2 Production of Silicon wafer for Solar Cell

Starting material for the production of Si is relatively pure sand which is also called quartzite and is reacted with carbon at high temperature in a furnace[14].

$$SiO_2 + 2C \longrightarrow Si + 2CO \qquad 1.1$$

This reaction gives metallurgical grade Si with purity having about 98%. Next the silicon is pulverized and treated with hydrogen chloride (HCl) to from trichlosilane:

$$Si + 3HCl \longrightarrow SiHCl_3 + H_2 \qquad 1.2$$

The purified $SiHCl_3$ is then used in a hydrogen reduction reaction to prepare the electronic grade silicon (EGS).

$$SiHCl_3 + H_2 \longrightarrow Si + 3HCl \qquad 1.3$$

Next these high purity but still polycrystalline EGS is converted to single crystal Si ingots or boules, this is typically done via Czochralski process (in which a Si seed crystal is pulled slowly out of a molten Si. Solidifying as it rises with the same crystal orientation as the seed). These ingots are then sawn into wafer and cleaned and polished which can then be processed into solar cells.

1.3 Solar Illumination

Fig. 1.1 depict the different solar spectra, the blackbody radiation at 6000 K, the extraterrestrial AM0 spectrum (the solar spectrum outside the earth's atmosphere) and the AM1.5 spectrum.

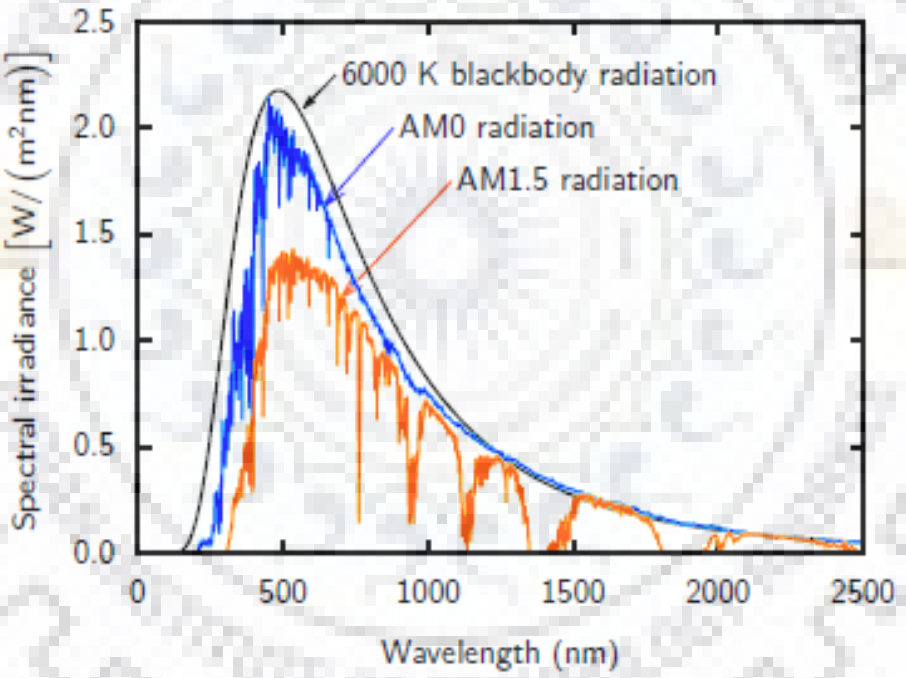

Figure 1.1 The different solar spectra[15]

When solar radiation travel through the atmosphere, it get attenuated by various factor such as due to water-vapor, absorption in the infrared, ozone absorption in the ultraviolet and scattering by airborne dust as shown in Fig. 1.1. The degree to which atmosphere affects the solar radiation received at the earth's surface is defined by the "Air Mass"(Fig 1.2).

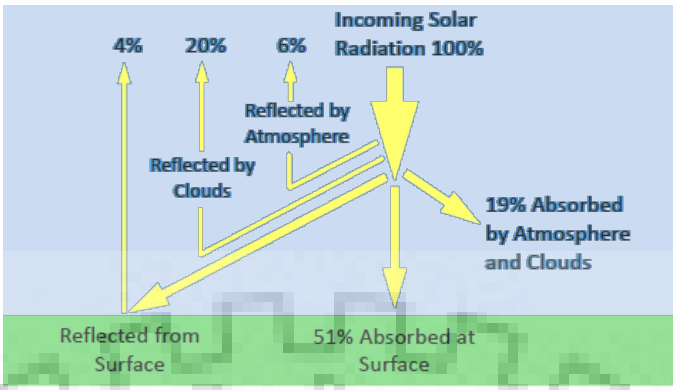

Figure 1.2 Source of solar radiation attenuation[16]

Air mass is defined as the secant of the angle between the sun and the zenith (sec Θ) and measures the atmospheric path length relative to the minimum path length when the sun is directly overhead.

$$AM = \frac{1}{\cos\theta} \tag{1.4}$$

Air Mass is followed by a number, which refers to the length of the path through the atmosphere in relation to the shortest length if the sun was in the apex.

The AM0 spectrum is relevant one for space vehicle and satellite application. Here, in our simulation study, we have used A.M1.5G solar spectrum." Air Mass 1.5" indicates that the solar light has been attenuated by passage through the earth's atmosphere a distance equal to 1.5 times the shortest path (which is when the sun is directly overhead). "Global" indicates that both direct and diffuse components of solar radiation are included.

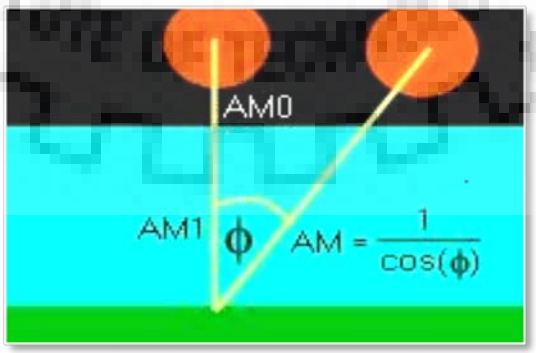

Figure 1.3 Schematic of air mass.

1.4 The p-n Junction under Illumination

When p-type and n-type semiconductor sandwiched together, forms a p-n junction. When this junction is illuminated (as shown in Fig. 1.4) electron-hole pair generated in semiconductor. The concentration of minority carriers (electron in the p-type region and holes in the n-type region) strongly increases. This excess photo generated minority carrier diffuse through the quasi-neutral region until they reach the p-n junction where drift caused by the built-in electric field separates the carries. The flow of the photo-generated carrier causes to the photo- generated current J_{ph}.

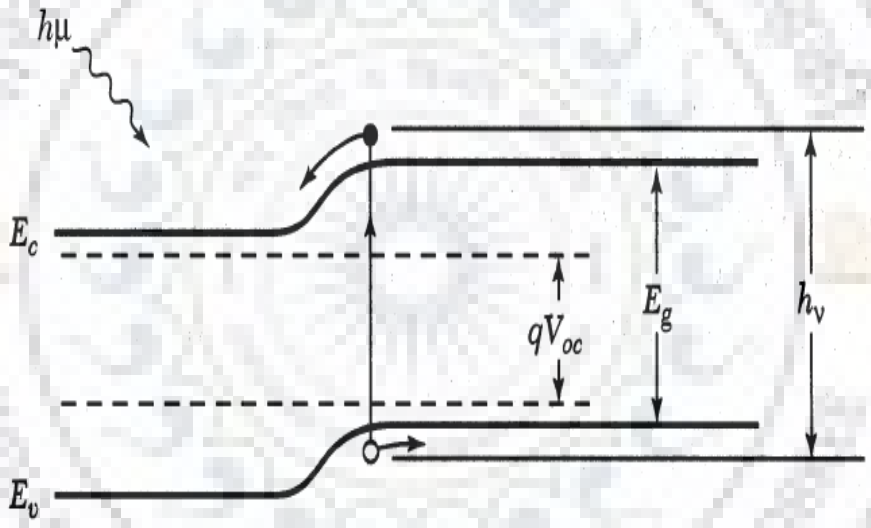

Figure 1.4 Band diagram of p-n junction[14]

The current- voltage curve provides the basics for the characterization of the solar cell performance. In an ideal cell, the current density J is equal the current density J_{ph} (photo current) minus the diode current density J_D

$$J = J_{ph} - J_D \quad (1.5)$$

$$J = J_{ph} - J_o\left(e^{qV/kT} - 1\right) \quad (1.6)$$

Both the dark and illuminated *J-V* characteristics of p-n junction are shown. The illuminated *J-V* characteristics (Fig. 1.5) of p-n junction is same as the dark *J-V* characteristics, but it is shifted down by the photo-generated current density J_{ph}.

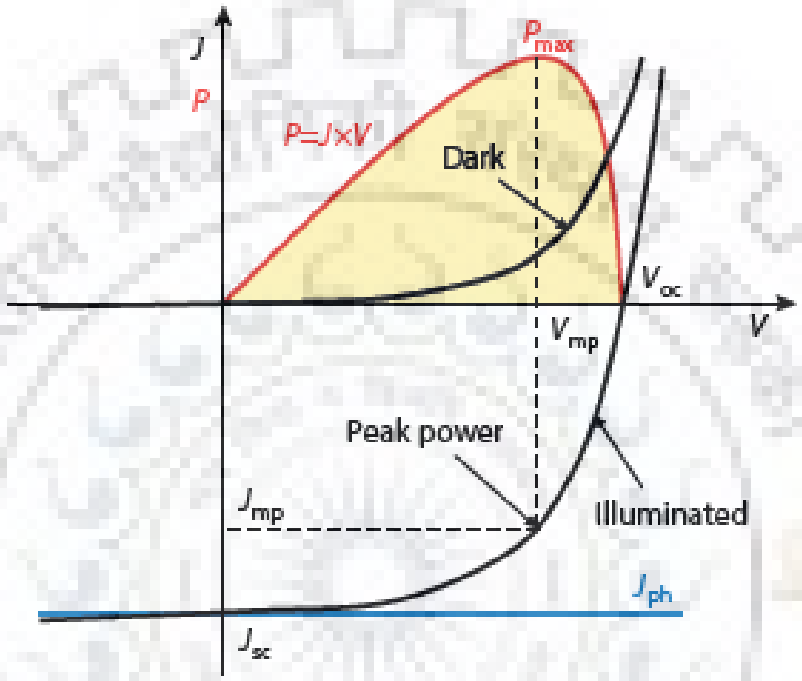

Figure 1.5 *J-V* characteristics of the p-n junction in the dark and under illuminated condition[15].

Chapter 2

Literature Review

2.1 Current Photovoltaic Technology

In recent years, tremendous emphasis is made to make the solar cell device, which is cost effective as well as giving high efficiency. For that reason nanostructure materials have been extensively explored for photovoltaic devices. Specifically, NW devices have been studied experimentally and computationally[17][18][19]. The use of NW in solar cell has been tried like in dye-sensitized solar cell[20], polymer based solar cell and hybrid organic and inorganic solar cell [21].

There has been significant work on the use of metal oxide wires in dye-sensitized solar cell (DSSC) configurations [22], although a number of studies have also used metal oxide NWs as charge collectors in hybrid organic/inorganic solar cells. Some novel structures are also been tried like single-crystalline n-CdS nanopillars, embedded in polycrystalline thin films of p-CdTe [23] and vertically aligned p-type single-crystalline GaN nanorod arrays on n-type Si for heterojunction photovoltaic cells[24], to enable high absorption of light and efficient collection of the carriers.

In addition, silicon NWs have also been used to change the reflective properties of silicon solar cells[13]. Large emphasis is made on growing NWs on different substrate like glass, aluminum[3]. For getting the high efficiency using the silicon NWs grown using VLS method, research is going around the world to make them defect free and catalyst contamination free [11], [12].

Conversion efficiency as high as 24% has been achieved with planar single junction silicon solar cell[25]. While, solar cell having 46% conversion efficiency has been demonstrated using multijunction concept[25].

The highest efficiency reported for vertical NW solar cell is around 6%[23] with CdS/CdTe structure. For lateral NW solar cell the best reported efficiency is around 4% with silicon co-

axial p-i-n structure[7].NW based solar efficiency can be further improved by proper analysis of fill factor, length and radius of NWs[26].

2.2 Advantages of NW Based Solar Cells

2.2.1 Orthogonalize Light Absorption and Carrier Transport[27]

Despite the several solar cell technology continuously decreasing the cost per kilowatt-hour of electricity generated but its cost is still too high to adopt it worldwide. So, the cost reduction in per kilowatt-hour has motivated us to radial junction solar cell which can be made on much lower quality silicon wafer without compromising the efficiency. Such lower quality of material have high defect density or high impurity level which reduces the diffusion length. Electron hole pair generated when photon falls on solar cell which are separated by the built in potential in planner solar cell. To generate electricity, these generated electron-hole pair must be able to traverse the thickness of cell. So, lower grade material used in planner p-n solar cell limit the charge collection because of lower diffusion length i.e. for planner solar cell with p-type base we must have

$$L_n > 1/\alpha$$

and,

$$L > 1/\alpha$$

Where L_n is the diffusion length of minority carrier in p type base, L is the thickness of Cell and $1/\alpha$ is optical thickness of material. Optical thickness is thickness of material to absorb 90% of incident photon with energy greater than the band gap energy. Silicon has optical thickness of 125μm. So, the material with diffusion length that are very low relative to the optical thickness cannot be readily used for high efficiency planner solar cell.

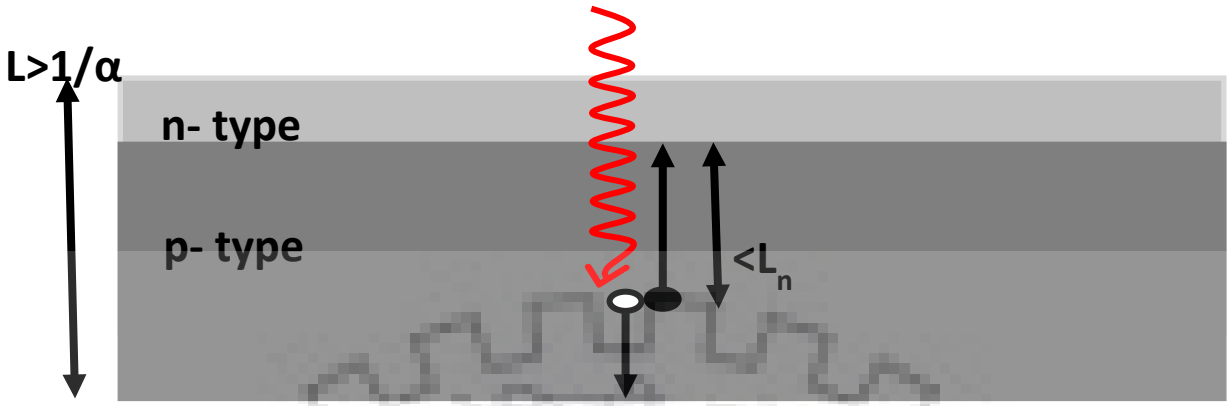

Figure 2.1 schematic of traditional planar solar cell device

Light absorption and charge extraction in orthogonal direction provide the potential solution for device design and optimization issue. The first such orthogonalize charge extraction device design was proposed by J.F. Wise in 1966 named “Vertical multijunction” solar cell[28]. Such type of structure propose allows the absorption of incident light parallel to the junction rather than in planner solar cell. The merit of such vertical junction lies in the fact

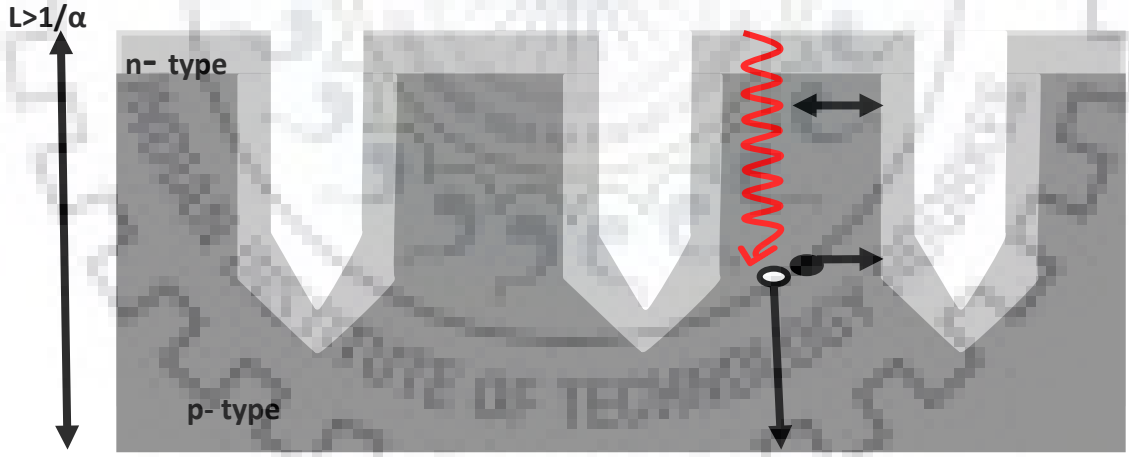

Figure 2.2 Schematic of vertical multi-junction solar cell device

that such type of junction has higher probability of collecting the photon generated minority carrier. Hence, improves charge collection efficiency.

2.2.2 Light Scattering Effect

Solar cell based on NW array is shown to have enhanced light absorption because of scattering[24]. Fig. 2.3 shows the schematic of NW array with light scattering effect. As the light travels through the NW array, it gets reflected by the NWs in turns increasing scattering and hence absorption, which eventually increases solar cell performance. The scattering of light in NW array is angle dependent as depicted in Fig. 2.3. This makes the NW array solar cell performance angle dependent.

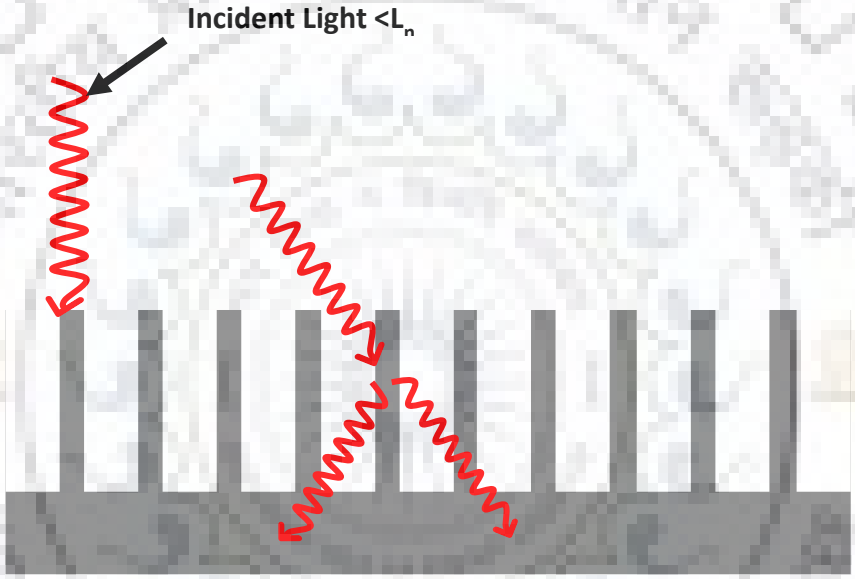

Figure 2.3 Schematic of NW array solar cell with light scattering effect.

2.2.3 Light Trapping Effect

It has been reported that there is a strong enhancement of the light absorption in single co-axial NW of silicon core/dielectric shells [10]. It has been found that there is a strong light trapping in silicon core because of the presence of dielectric shells. This enhancement in light trapping is basically due to the off-resonance enhancement, which strongly depends upon the core radius, the shell thickness and the shell refractive index.

Fig. 2.4 shows the schematic coaxial NW, where yellow (blue) stands for silicon core (shell), m_0 (air), m_1 (shell) and m_2 (core) are the refractive index.

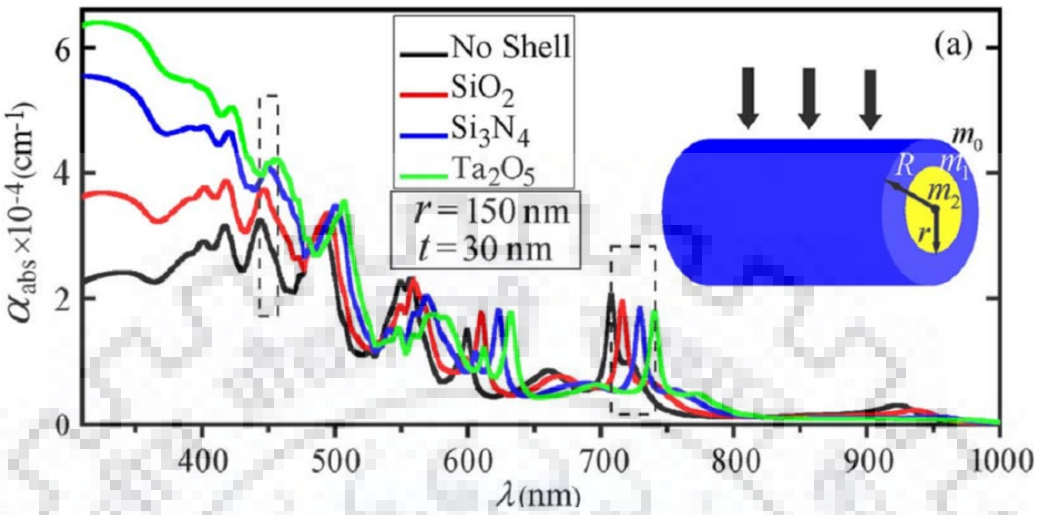

Figure 2.4 Schematics of coaxial NW with light trapping effect [10].

2.2.4 High Surface Area

NW has high surface area, although high surface area is not good for solid state solar cell because it increases the surface recombination, which degrades solar cell performance. But in case of dye-synthesized solar cell this high surface is useful and provide direct pathway for rapid collection of charge carrier generated throughout the solar cell.

2.2.5 Wider Range of Materials/Heterostructures

Another advantage of using NWs is that wider range of materials can be used in fabricating multijunction solar cells [18]. This is because, NWs can withstand higher strain as compare to thin film, which allows us to use the different combination of materials to fully utilize the solar spectrum.

2.2.6 High Built-in Electric Field

NW structure has higher built-in electric field that arises because of its radial geometry. This higher electric field as compare to its planar counterpart plays very important role in efficient and rapid collection of generated electron-hole pairs.

2.3 The Nano/Micro wire Array solar Cell

We proposed here the p-n junction radial nanowire array solar cell i.e. this device consisting of semiconductor nanowire each with radial p-n junction. Which gives the potential benefit of maintaining the short minority carrier transport distance in an optically thick cell with low cost method which allows to grow nanowire at room temperature without using sophisticated instrument. Such an array of nano- or microwires with p-n junction in radial direction allows the decoupling of requirement for absorption of light and carrier extraction in orthogonal direction. Each individual wire forming p-n junction could be long enough in the direction of incident of light which allows the optimal light absorption but thin in other direction hence increases the charge collection efficiency. Theoretical and experimental exploration of radial p-n junction solar cell design is topic of this thesis.

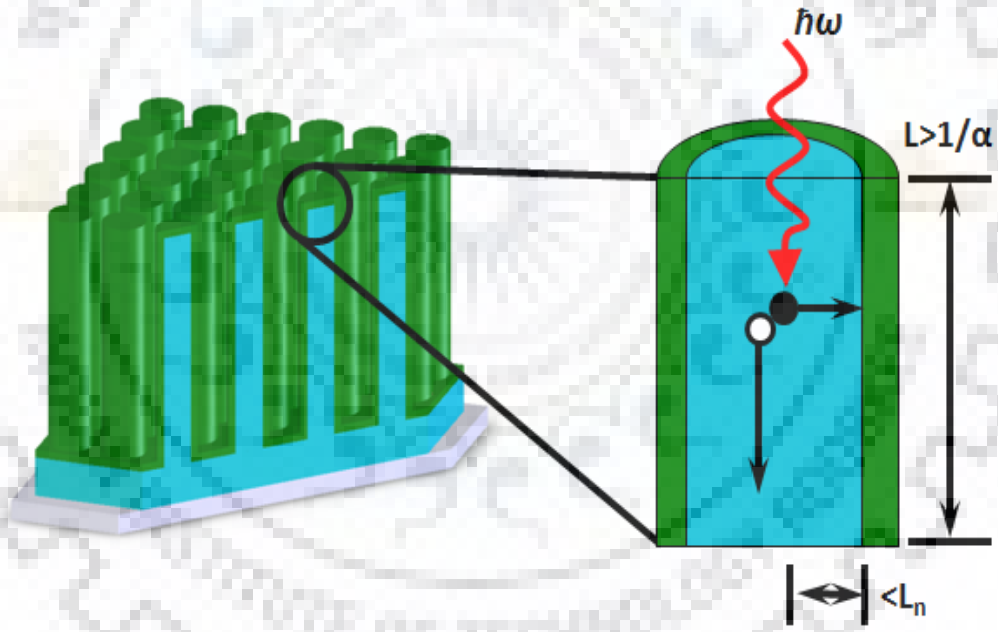

Figure 2.5 Schematic of radial junction array[27]

Chapter 3

Physics of Solar Cell Device and Radial p-n Junction

3.1 Introduction

This chapter will begin with basic concept of solar cell which provide motivation for the radial p-n junction followed by the comparison between the efficiency of planner and radial junction solar cell. Further, we discuss the how impurity concentration place a major role to control the width of depletion layer so that nanowire is not completely depleted.

3.2 Salient Features

Efficiency η, of solar cell is define as the ration of total electrical output power P_{out} divided by the total incident optical power P_{in} under 1.5G illumination [29]

$$\eta = \frac{P_{out}}{P_{in}} \tag{3.1}$$

$$= \frac{V_{oc} \times J_{sc} \times FF}{P_{in}} \tag{3.2}$$

Where

V_{oc} = Open circuit voltage when across the cell when no current is flowing

J_{sc} = Short circuit current density at zero bias

FF = the fill factor which is the ration of maximum electrical output power to the product of V_{oc} and J_{sc}

Efficiency of planner solar cell decreases as the diffusion length of minority carrier decreases so as open circuit voltage, short circuit current density and fill factor decrease.

Now, if we consider a solar cell as an ideal p-n diode so the light generated current equation[15] can be written as

$$J = J_{sc} - J_o \left[exp\left(\frac{qV}{k_B T}\right) - 1 \right] \tag{3.3}$$

Under open circuit condition i.e. J=0, we can have V_{oc}

$$V_{oc} = \frac{k_B T}{q} ln\left[\left(\frac{J_{sc}}{J_o}\right) + 1\right] \quad (3.4)$$

$$\approx \frac{k_B T}{q} ln\left(\frac{J_{sc}}{J_o}\right) \quad (3.5)$$

Where

q= 1.602193X10^{-19}C is the magnitude of electron charge

k_B= 1.38073X10^{-23} m^{2}kgs^{-2}K^{-1} is Boltzmann's constant

T= it is assumed to be 300 K.

Now, we will treat the minority carrier diffusion length L_n (or L_p for hole) as a quantity which judges the quality of material. This quantity is the measure of average distance travelled by the carrier from the point of generation before it recombines. Diffusion length is related to carrier lifetime and mobility by the following expression[27]:

$$L_n = \sqrt{D_n \tau_n} \quad (3.6)$$

$$= \sqrt{\frac{k_B T \mu_n \tau_n}{q}} \quad (3.7)$$

Similar expression holds for the holes. Now, the recombination processes is dominated by the recombination through mid-gap trap i.e. Shockley Read Hall recombination, so the minority carrier lifetime can be related to the trap density:

$$\tau_{n0} = \frac{1}{\sigma_n N_r v_{th}} \quad (3.8)$$

Where

σ_n = Cross section area of electron capture

N_r = density of recombination center

v_{th} = Thermal velocity

Again, similar expression holds for holes

J_{sc} is considered as the number of light generated minority carrier that are swept across the junction per unit time, assuming ideal minority carrier transport and collection. So, we can

expect that the J_{sc} will increase and the L_n increases, until some limiting value, when either the L_n become much larger than the cell thickness, or much larger than the optical thickness of material.

To get a motivation for the potential benefit of radial p-n junction with an intuitive model to describe the effect of reducing diffusion length in PV device, let us assume a optically thick (i.e. 125 μm thick) Si PV device with a p-type base material and negligible thin emitter, insignificant surface recombination , and baseline parameter of the record Si solar cell (the UNSW PERL cell[25]) , namely J_{sc} = 0.0422 A/cm^2 ,V_{oc} = 0.706 V, and Fill Factor = 0.828 so that η = 24.7%. this means we get Jo ≈ 5.8X10^{-14} A/cm^2 from above written eq. 3.3 Then consider the effect of reducing the minority diffusion length L_n. Assume that carrier generation per unit volume is independent of depth into the cell, all that carrier generate within the L_n of the p-n junction are collected and rest get recombine i.e. for planner geometry assume that[30]:

$$J_{sc} = 0.0422 \times \frac{L_n}{L}, \quad L_n \leq L \tag{3.9}$$

Where Jsc is in A/cm^2, L_n is minority electron diffusion length and L is cell thickness. Then we can calculate the V_{oc} and J_{sc} from the eq. 2.10 and eq. 2.9 Assuming that the Fill Factor is not affected by the change in L_n.

In radial junction geometry we assume the nanowire as the shape of cylinder. As the charge collection is in orthogonal direction to the incident light so the radius of cylinder is set to the equal of minority diffusion length and carrier generated within the L_n of p-n junction get collected. Hence, J_{sc} is independent of L_n and V_{oc} can be calculated by the following expression[30]:

$$V_{oc} = \frac{k_B T}{q} ln\left[\left(\frac{J_{sc}}{J_0 \acute{y}}\right) + 1\right] \tag{3.10}$$

Where $\acute{y}$ is area of p-n junction in cylindrical geometry relative to the area of the top of the cylindrical geometry. Again, efficiency can be calculate by eq. 3.2 the result of simple comparison of both the geometry is given in the table

Table 3.1 Comparison of the basic feature of the planar and radial geometry[30]

	L_n	125	100	10	1
Planar Cell	J_{sc} (A/cm^2)	0.0422	0.0338	0.00338	0.00038
	V_{oc}	0.706	0.700	0.641	0.581
	FF	0.828	0.828	0.828	0.828
	Efficiency (%)	24.7	19.6	1.8	0.2
Radial junction cell	Junction area increase	3	3.5	26	251
	J_{sc} (A/cm^2)	0.042	0.0422	0.0422	0.0422
	V_{oc}	0.678	0.674	0.622	0.563
	FF	0.828	0.828	0.828	0.828
	Efficiency (%)	23.7	23.5	21.7	19.7

The above oversimplified solar cell principles intuitively demonstrates the potential advantage of radial geometry over the planner geometry. It is clear from the table as the minority carrier diffusion decreases which is in the case of high trap density or due to the high impurity, decreases the efficiency drastically but in radial geometry still good efficiency can be achieved by using low grade silicon material. It is because the light generated minority carrier travel along the radius of the geometry and collection is guaranteed for the carrier within the diffusion length of the junction. For simplification we have neglected to treat the effect of emitter, the wire surface, and the p-n junction region also we have ignored the any issue associated with the inevitably less than 100% packing fraction that we will have in radial geometry.

Nevertheless, this simple analysis does point out some key feature associated with the novel geometry. The radial junction show much higher tolerance to reduced diffusion length than the planner geometry, it is because the ability to retain the higher charge collection which is independent of the diffusion length. This is paid by the reduction in V_{oc} by increase in the higher area, but it is logarithm dependence it is a lesser effect.

3.3 Recombination Losses

The performance of solar cell is limited by the recombination process that occurs in the solar cell, which basically reduces the effective collection of charge carrier.

There are following recombination processes that limit the charge collection efficiency of a solar cell.

3.3.1 Shockley Read Hall Recombination

It is the dominant form of recombination mechanism in most of the solar cells. In this type of recombination due to the impurities present in the semiconductor an additional energy level is introduce within the forbidden energy gap. This energy level acts as a trap and captures electrons and holes, leading to recombination.

The relationship between recombination rate (U) (in unit of cm^{-3}/s) and trap density (N_t) (in unit of cm^{-3}) is given by relation [15].

$$U = \frac{\sigma_p \sigma_n v_{th} (pn - {n_i}^2) N_t}{\sigma_n \left[n + n_i exp\left(\frac{E_t - E_i}{kT}\right)\right] + \sigma_p \left[p + n_i exp\left(\frac{-(E_t - E_i)}{kT}\right)\right]} \quad (3.11)$$

Where,

σ_p = hole capture cross-section, n_i = intrinsic carrier density, v_{th} = thermal velocity

σ_n =electron capture cross-section, E_i = intrinsic energy level, N_t = trap density

3.3.2 Band to Band Recombination

It is a radiative form of recombination in which an electron from conduction band recombines with the hole in the valence band with emission of energy [15]. Band to band recombination mainly occurs in direct band gap semiconductors. The probability of occurrence of this form of recombination in indirect band gap semiconductor is very low.

3.3.3 Auger Recombination

This type of recombination occurs in heavily doped semiconductors. In this recombination mechanism hole from the valence band recombines with the electron in the conduction band. The excess energy released during this recombination is absorbed by the neighboring electron in the conduction band, which then goes to some higher energy level and then again falls back to the conduction band with release of energy[15].The Fig. 3.1 shows all three kinds of recombination discussed above

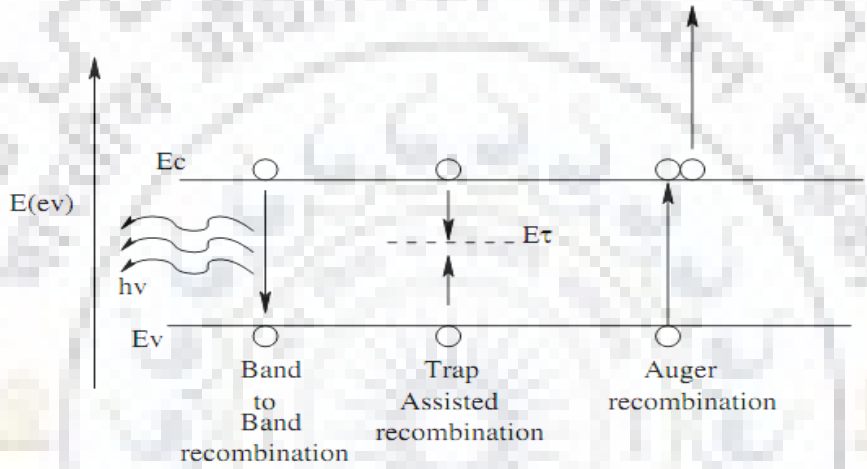

Figure 3.1 Schematic of different kind of recombination in a typical solar cell.

3.3.4 Surface Recombination

Because of abrupt termination of crystal structure, semiconductor surface has large number of dangling bonds. These dangling bond acts as recombination centers for charge carriers. Carriers generated near the surface fall in to these dangling bonds and gets recombine.

3.4 Effect of Doping on Radial Junction

Let us consider relatively thick an abrupt radial p-n junction of several 100 nm diameter (quantum size effect is neglected) with core radius R_1 having impurity concentration N_A and outer shell of thickness R_2- R_1 with impurity concentration of N_D as shown in Fig. 3.2

The r axis can be divided in four region namely[31]

- The quasi neutral part of core r<= R_1-w_p
- The depletion region in core thickness w_p
- The quasi neutral region in outer shell R_1+w_n<=r<=R_2
- The depletion region in shell of width w_n

When a p-n junction is formed along radial direction then the majority charge carrier from p side i.e. from core will flow toward n side i.e. toward shell and majority charge carrier from n side will flow towards p side an as a result forming a space charge region at the core-shell interface and potential energy barrier is established.

That built in potential energy barrier that forms along the p-n junction has height defined by the work function difference of the core and shell, can be written as

$$\varphi_o = kTln\frac{n_n p_p}{n_i^2} \tag{3.12}$$

Where kT is the thermal energy, n_i is the intrinsic carrier concentration of the semiconductor. At thermal equilibrium the total electron current and total hole current flow is zero.

The space charge is mainly formed by ionized donors and acceptor. In complete depletion approximation the space charge density is:

$$\rho = \begin{cases} -eN_A = -e.p_p \,; R_1 - w_p \le r \le R_1 \\ eN_D = e.n_n \,; R_1 \le r \le R_1 + w_n \end{cases} \tag{3.13}$$

To determine the potential distribution across the junction, we should solve the Poisson equation in cylindrical coordinate:

$$\frac{1}{r}\frac{d}{dr}\left(r\frac{d\varphi}{dr}\right) = \begin{cases} -\frac{e^2 p_p}{\varepsilon\varepsilon_0}, & R_1 - w_p \le r \le R_1 \\ \frac{e^2 n_n}{\varepsilon\varepsilon_0}, & R_1 \le r \le R_1 + w_n \end{cases} \tag{3.14}$$

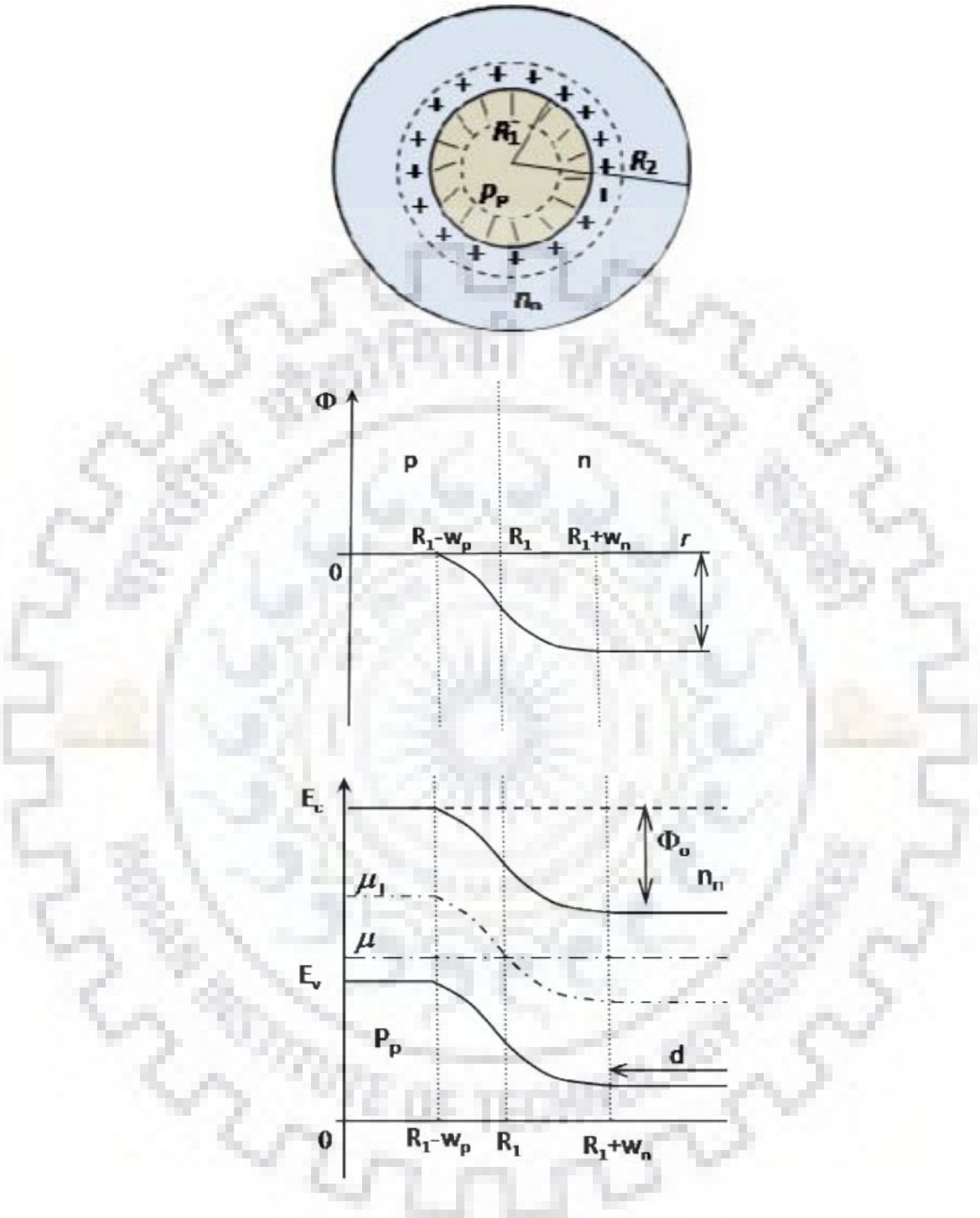

Figure 3.2 Cross cestion of core/shell nanowire , profile of potentioal across the junction and energy band diagram respectively[31]

Where φ the potential energy of electron is, ε is the permittivity of the semiconductor, ε_0 is the electric constant. The radial component of the electric field should be zero outside the space charge region:

$$\varphi(R_1 - w_p) = 0, \quad \frac{d\varphi}{dr}\Big| r = R_1 - w_p = 0 \tag{3.15}$$

$$\varphi(R_1 + w_n) = -\varphi_0, \quad \frac{d\varphi}{dr}\Big| r = R_1 + w_n = 0 \tag{3.16}$$

Solution for the eq. 3.14 – 3.16 has the form

$$\varphi(r) = -\frac{e^2 p_p}{4\varepsilon\varepsilon_0}\left[r^2 - (R_1 - w_p)^2 - 2(R_1 - w_p)^2 ln\frac{r}{R_1 - w_p}\right] \; for\; R_1 \le r \le R_1 \tag{3.17}$$

And

$$\varphi(r) = \varphi_0 + \frac{e^2 n_n}{4\varepsilon\varepsilon_0}\left[r^2 - (R_1 + w_n)^2 - 2(R_1 + w_n)^2 ln\frac{r}{R_1 + w_n}\right] \; for\; R_1 \le r \le R_1 \tag{3.18}$$

In this model charge on core/shell interface states is ignored, so the electric field at r= R_1 gives

$$n_n(R_1^2 - (R_1 + w_n)^2) = p_p((R_1 - w_n)^2 - R_1^2) \tag{3.19}$$

Which represents the charge neutrality of the junction. Using eq. 2.18 and 2.19 and demanding the continuity of the potential at the junction interface r=R_1. We get the following equation for w_p-

$$\left(\frac{n_n + p_p}{p_p} - \left(1 - \frac{w_p}{R_1}\right)^2\right).ln\left(\frac{n_n + p_p}{n_n} - \frac{p_p}{n_n}\left(1 - \frac{w_p}{R_1}\right)^2\right) + \left(1 - \frac{w_p}{R_1}\right)^2 ln\left(1 - \frac{w_p}{R_1}\right)^2 = \frac{4\varepsilon\varepsilon_0}{\varepsilon^2 p_p {R_1}^2}\varphi_0 \tag{3.20}$$

Thus for the given n_n, p_p, φ_0 and R_1 the depletion width in the core and the shell can be calculated from eq. 3.19 and 3.20.

It is worth to note that in the radial junction the width of space charge layer is a function of the core radius, this means that for the NWs with the same doping level but different radius the depletion layers has the different width.

As it follows from eq. 3.19 the ration of w_p/w_n depends not only on the doping concentration but also on the NW radius.

$$\frac{w_p}{w_n} = \frac{n_n}{p_p}\frac{2+\frac{w_n}{R_1}}{2-\frac{w_n}{R_1}} \tag{3.21}$$

It is evident from the equation that at equal core and shell doping levels the depletion width in the core is always larger than in the shell.

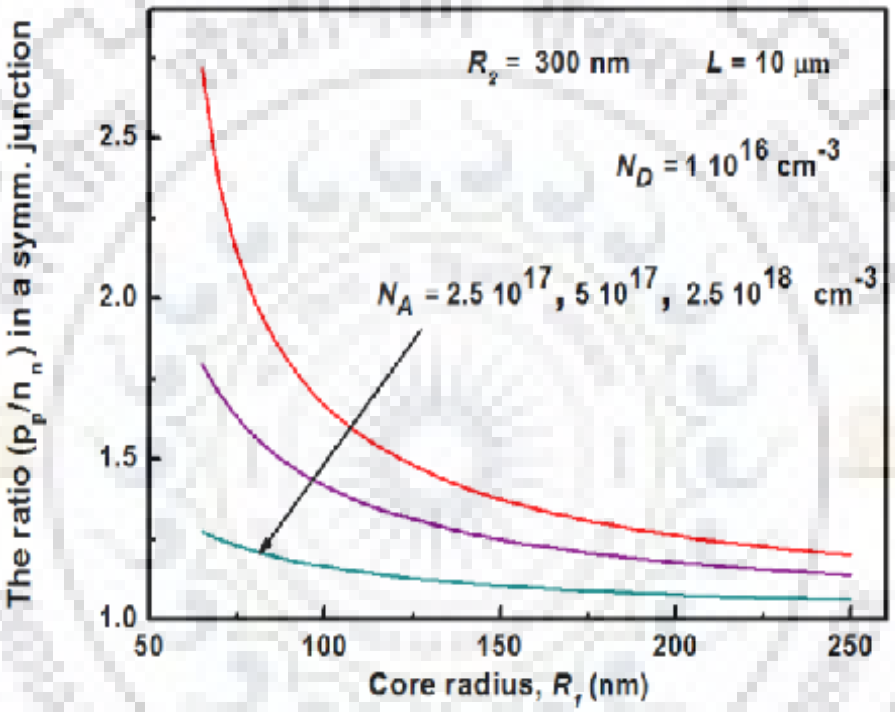

Figure 3.3 Effect of doping concentration on core radius[31].

Chapter 4

MATLAB simulation of the Radial p-n Junction Solar Cell

4.1 Transportation Equation in the Radial Geometry

In order to understand how the radial junction geometry perform relative to the planar geometry, Carrier transport equation is necessary to solve in cylindrical coordinate system. Let us consider a core/shell nanowire cylinder which can be divided into four region[30] as shown in Fig. 4.1

- The quasineutral part of the n-type emitter region (of width x_1)
- The depletion region of the n-type material (of width x_2)
- The depletion of the p-type material (of width x_3)
- The quasineutral part of the p-type material (of width x_4)

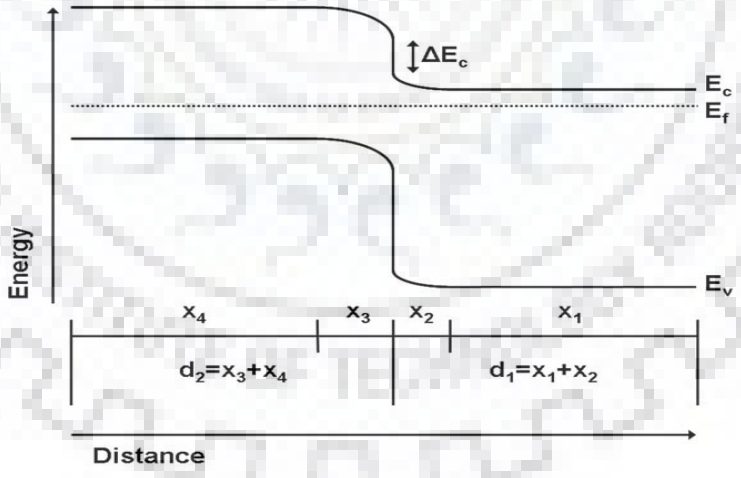

Figure 4.1 Generalize band structure for p-n heterojunction structure[30].

The p-n junction in each wire was assumed to be abrupt, and depletion approximation was invoked. The emitter layer (i.e. shell of the wire) was assumed to be n-type and the base (i.e.

the core of the wire) was assumed to be p-type as shown in Fig. 4.2. The analogous schematic for the planar structure is shown in Fig. 4.3.

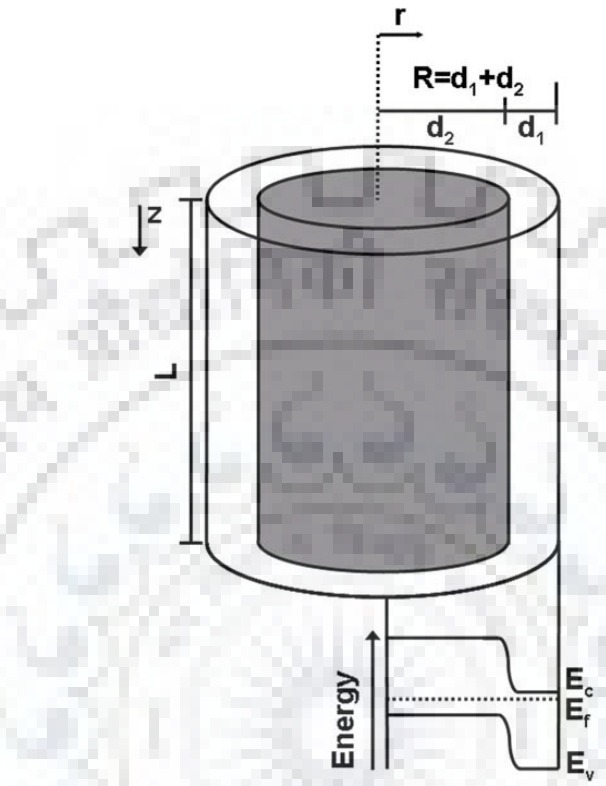

Figure 4.2 Schematic of single wire from the radial p-n junction cell, and corresponding energy band diagram[30]

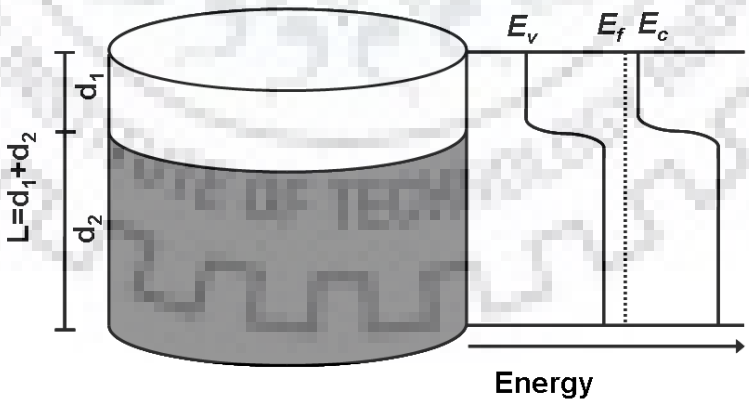

Figure 4.3 A conventional planar solar cell and its band diagram[30].

Light was assumed to be normally incident on the top face of the wire, with no reflection. Recombination was assumed to be purely due to the Shockley-Read-Hall recombination. Auger recombination were neglected. However, Surface recombination effects were included by assuming a minority carrier surface recombination velocity S at the r=R surface.

4.1.1 Quasineutral Regions

In analogy to treatment of planar p-n junction the minority carrier movement in the quasineutral region of the p-type base material was to be governed by the transport equation[30],

$$\nabla^2 n' - \frac{n'}{{L_n}^2} = \frac{\partial^2 n'}{\partial r^2} + \frac{1}{r}\frac{\partial n'}{\partial r} - \frac{n'}{{L_n}^2} = -\frac{\alpha_2 \Gamma_0}{D_n} e^{\alpha_2 z} \tag{4.1}$$

Where n' = n - n_o is the excess minority electron concentration with respect to the equilibrium value n_0. L_n is the diffusion length of the minority electron, α_2 is the absorption coefficient of the p-type material, $\boldsymbol{\Gamma}_0$ is the incident photon flus and D_n is the electron diffusion coefficient. The boundary conditions are

$$n'(0) = finite \tag{4.2}$$

$$n'(x_4) = n_0\left(e^{qV/k_B T} - 1\right) \tag{4.3}$$

Where V is the applied bias, and the T is assumed to be 300 K. The current density in the p-type quasineutral region, J^P, is thus

$$J^p = \frac{2x_4 \int_0^L J^p(z)dz}{R^2} \tag{4.4}$$

Where

$$J^p(z) = -qD_n \frac{\partial n'}{\partial r}\Big|_{r=x_4} \tag{4.5}$$

And R and L are the radius and length of the wire, respectively.

In the quasineutral region of the n- type emitter, the transport equation is

$$\frac{\partial^2 p'}{\partial r^2} + \frac{1}{r}\frac{\partial p'}{\partial r} - \frac{p'}{{L_p}^2} = -\frac{\alpha_1 \Gamma_0}{D_p} e^{\alpha_1 z} \tag{4.6}$$

Where p' = p- p_0 is the excess minority hole concentration with respect to the equilibrium value p_0, L_p is the diffusion length of minority holes, α_1 is the absorption coefficient of the n-type material and D_p is the minority hole diffusion coefficient.

The boundary conditions were

$$p'(R - x_1) = p_0\left(e^{qV/k_BT} - 1\right) \tag{4.7}$$

$$-S_p \mathrm{p'(R)} = -D_p \left.\frac{\partial p'}{\partial r}\right|_{r=R} \tag{4.8}$$

Where S_p is the surface recombination velocity of the holes at the external surface of the wire. Hence, we get the current density in the n-type quasineutral region, J^n, is

$$J^n = \frac{2(R - x_1)\int_0^L J^n(z)dz}{R^2} \tag{4.9}$$

Where

$$J^z(z) = qD_p \left.\frac{\partial p\prime}{\partial r}\right|_{r=R=x_1} \tag{4.10}$$

4.1.2 Depletion Region

By solving the Poisson's equation for the depletion region, the width of the depletion region can be obtained, assuming that outside the depletion region the electric field is zero and the εE is continuous across the junction, where ε is the dielectric constant of the semiconductor, and that ionized donors and acceptor were the main constituents charge.

The J_g^{dep} , which is light generated current density can be calculated by assuming that all of the incident that was absorbed participate in production of carriers that were collected. Hence, in the p-type part of the depletion region

$$J_g^{dep,p}(V) = q\Gamma_0\,(1 - e^{-\alpha_2 L})\frac{{d_2}^2 - {x_4}^2}{R^2} \tag{4.11}$$

Whereas in the n-type part of the depletion region

$$J_g^{dep,n}(V) = q\boldsymbol{\Gamma_0}\,(\mathbf{1} - \boldsymbol{e^{-\alpha_1 L}})\frac{(\boldsymbol{{d_2}^2 + {x_4}^2})^2 - \boldsymbol{{d_2}^2}}{\boldsymbol{R^2}} \tag{4.12}$$

4.2 Equation Solution

If we the solve the above equation with the stated assumption gives the following expression for the J-V behavior of the device[30]:

$$J = J_0^p + J_0^n\left(e^{qV/k_BT} - 1\right) - J_l^p - J_l^n + J_r^{dep}(V) - J_g^{dep,p}(V) - J_g^{dep,n}(V) \tag{4.12}$$

Where

$$J_0^p = -2qn_0L\frac{D_n}{{L_p}^2}\frac{\beta_5}{{\beta_1}^2}\frac{I_1(\beta_5)}{I_0(\beta_5)} \tag{4.13}$$

$$J_0^n = -2qp_0L\frac{D_p}{{L_p}^2}\frac{\beta_2}{{\beta_1}^2}\left(\frac{f_1K_1(\beta_2) - f_2I_1(\beta_2)}{f_1K_0(\beta_5) + f_2I_0(\beta_2)}\right) \tag{4.14}$$

$$J_l^p = -2q\Gamma_0\frac{{L_n}^2}{{L_p}^2}\frac{\beta_5}{{\beta_1}^2}\frac{I_1(\beta_5)}{I_0(\beta_5)}\,(1 - e^{-\beta_6}) \tag{4.15}$$

$$J_l^n = -2q\Gamma_0\frac{\beta_2}{{\beta_1}^2}\left(\frac{K_1(\beta_2)(f_1 - \beta_4I_0(\beta_2)) - I_1(\beta_2)(f_2 + \beta_4K_0(\beta_2))}{f_1K_0(\beta_2) + f_2I_0(\beta_2)}\right) \times (1 - e^{-\beta_3}) \tag{4.16}$$

$$J_g^{dep,p}(V) = -q\Gamma_0\frac{{d_2}^2 - {x_4}^2}{R^2}\left(1 - e^{-\beta_6}\right) \tag{4.17}$$

$$J_g^{dep,n}(V) = -q\Gamma_0\frac{({d_2}^2 + {x_4}^2)^2 - {d_2}^2}{R^2}\left(1 - e^{-\beta_3}\right) \tag{4.18}$$

$$J_r^{dep}(V) = -qLU_{max}\frac{{r_2}^2 - {r_1}^2}{R^2} \tag{4.19}$$

Where $I_n(x)$ and $K_n(x)$, n=0 or 1, represent modified Bessel's function of the first and second kinds, respectively

The dimensionless parameters are defined as

$$\beta_1 = \frac{R}{L_p} \tag{4.20}$$

$$\beta_2 = \frac{R - x_1}{L_p} \tag{4.21}$$

$$\beta_3 = \alpha_1 L \tag{4.22}$$

$$\beta_4 = \frac{L_p S_p}{D_p} \tag{4.23}$$

$$\beta_5 = \frac{x_4}{L_n} \tag{4.24}$$

$$\beta_6 = \alpha_2 L \tag{4.25}$$

$$f_1 = f_1(\beta_1, \beta_4) = I_1(\beta_1) + \beta_4 I_0(\beta_1) \tag{4.26}$$

$$f_2 = f_2(\beta_1, \beta_4) = K_1(\beta_1) + \beta_4 K_0(\beta_1) \tag{4.27}$$

Additionally

$$U_{max} = \frac{n_{i,*}}{\sqrt{\tau_{n0}\tau_{p0}}} \sinh\left(\frac{qV}{2k_B T}\right) \tag{4.28}$$

$$r_1(V) = r(V) - \frac{\left(x_2(V) + x_3(V)\right)}{2}\kappa \tag{4.29}$$

$$r_2 = r(V) + \frac{(x_2(V) + x_3(V))}{2}\kappa \tag{4.30}$$

$$r(V) = x_4 + \frac{log\left(\frac{N_a}{n_{i,p}}\right)}{log\left(\frac{N_a N_d}{n_{i,p} n_{i,n}}\right)}(x_2(V) + x_3(V)) \tag{4.31}$$

$$\kappa = \frac{\pi k_B T}{q(V_{bi} - V)} \tag{4.32}$$

$$V_{bi} - V = \frac{qN_d}{2\epsilon_n}(d_2 + x_2)^2 log\left(\frac{d_2 + x_2}{d_2}\right) + \frac{qN_d}{4\epsilon_n}\left[{d_2}^2 + (d_2 + x_2)^2\right] + \frac{qN_a}{2\epsilon_p}{x_4}^2 log\left(\frac{x_4}{d_2}\right) + \frac{qN_a}{4\epsilon_p}\left({d_2}^2 - {x_4}^2\right) \quad (4.33)$$

Where N_a, $n_{i,p}$, ϵ_p and τ_{n0} are the dopant (acceptor) density , intrinsic carrier concentration, dielectric constant and lifetime in the depletion region, respectively, for the p-type material. Similarly, N_d, $n_{i,n}$, ϵ_n, and τ_{p0} are analogous quantity for the n-type material. Also $n_{i,*}=n_{i,p}$ or $n_{i,n}$, depending upon whether the maximum recombination point lies in the p-type or n-type material. From Eq. 2.33 x_2(V) and x_3(V) can be found numerically, given the built-in voltage V_{bi}:

$$V_{bi} = \frac{k_B T}{q} log\left(\frac{N_a N_d}{n_{i,p} n_{i,n}}\right) + \frac{\Delta E_c}{q} \quad (4.34)$$

Where ΔE_c is the conduction band offset (=0 for homojunctions).

4.3 MATLAB Results

The above analytically achieved equation were written in MATLAB R2010a 32 bit version (MATLAB code given in appendix) and 3D graph. The obtain result were simulated for the radius up to 2 µm and length up to 100 µm. V_{oc}, J_{sc}, FF and efficiency were received for the various combination of dopant concentration, radius and length of nanowire.

Let us see some of the result obtain:

(A) For $N_a=N_d = 10^{14}$ cm^{-3}

(a) (b)

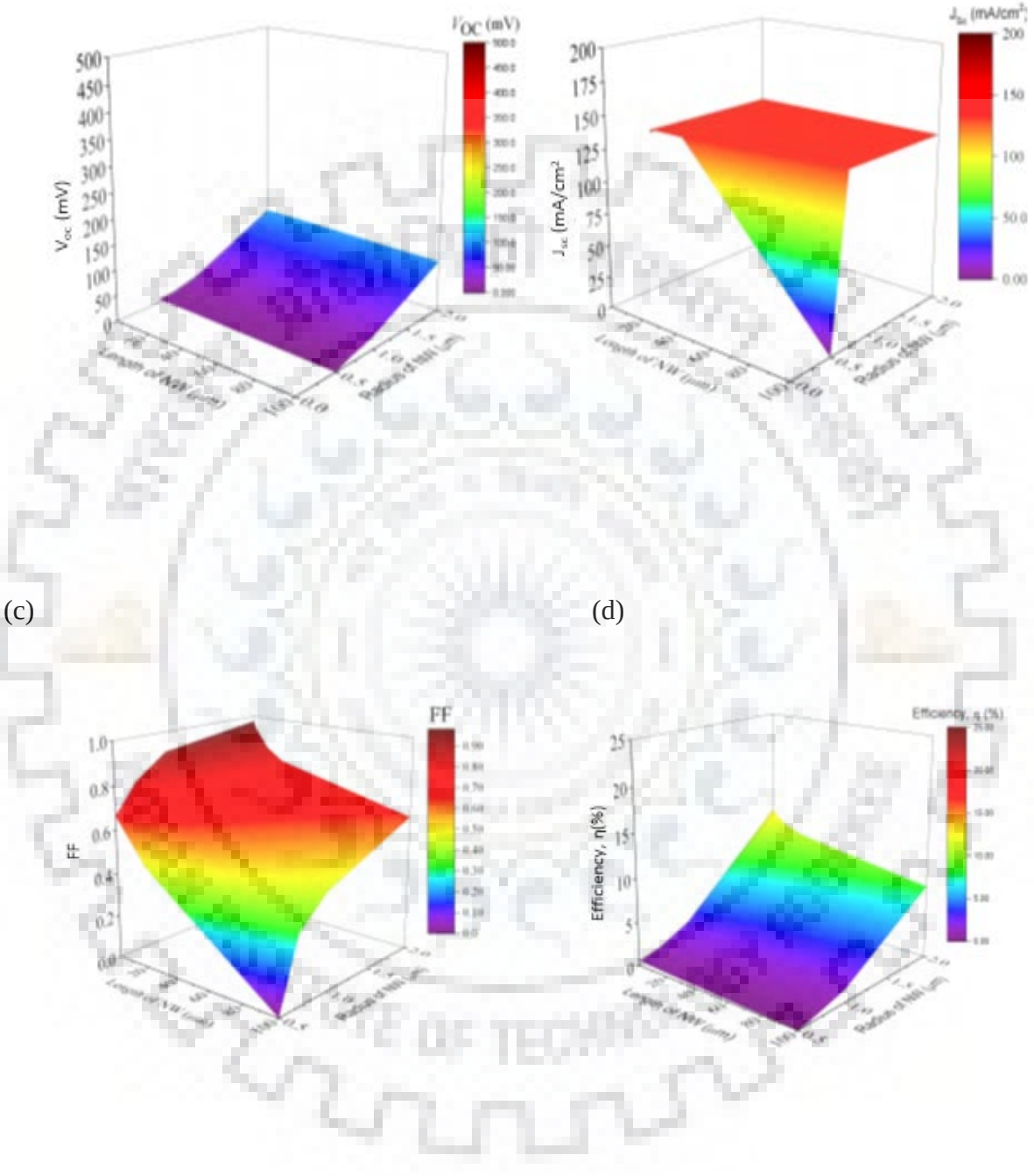

(c) (d)

Figure 4.4. MATLAB simulated graph for $N_a=N_d = 10^{14}$ cm^{-3} (a)V_{oc}, (b) J_{sc} (c) FF (d) Efficiency

(B) For $N_a=10^{14}$ cm^{-3} and $N_d=10^{15}$ cm^{-3}

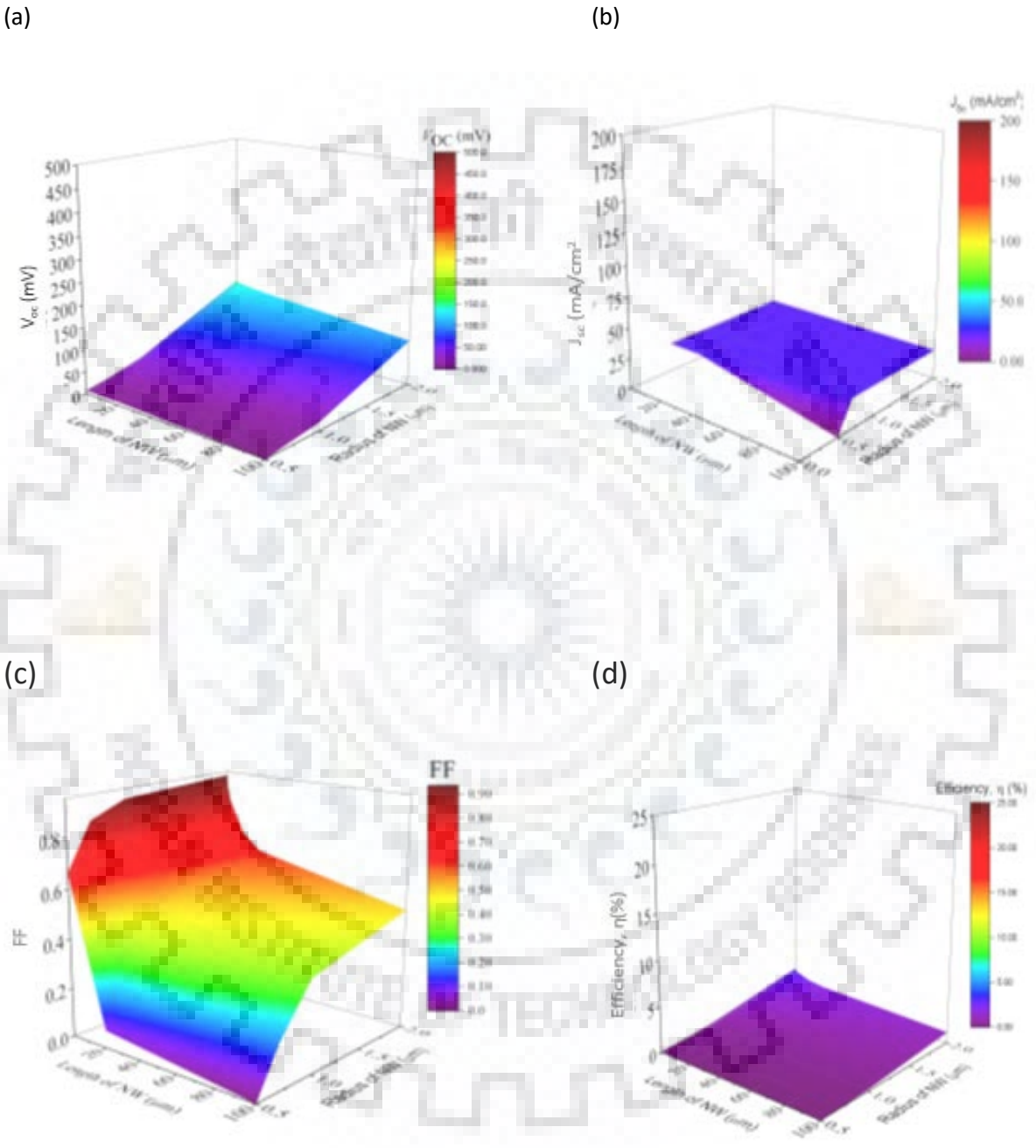

Figure 4.5 MATLAB simulated graph for $N_a=10^{14}$ cm^{-3} and $N_d=10^{15}$ cm^{-3}

(a)V_{oc}, (b) J_{sc} (c) FF (d) Efficiency

(C) For $N_a=10^{14}$ cm^{-3} and $N_d=10^{16}$ cm^{-3}

(a) (b)

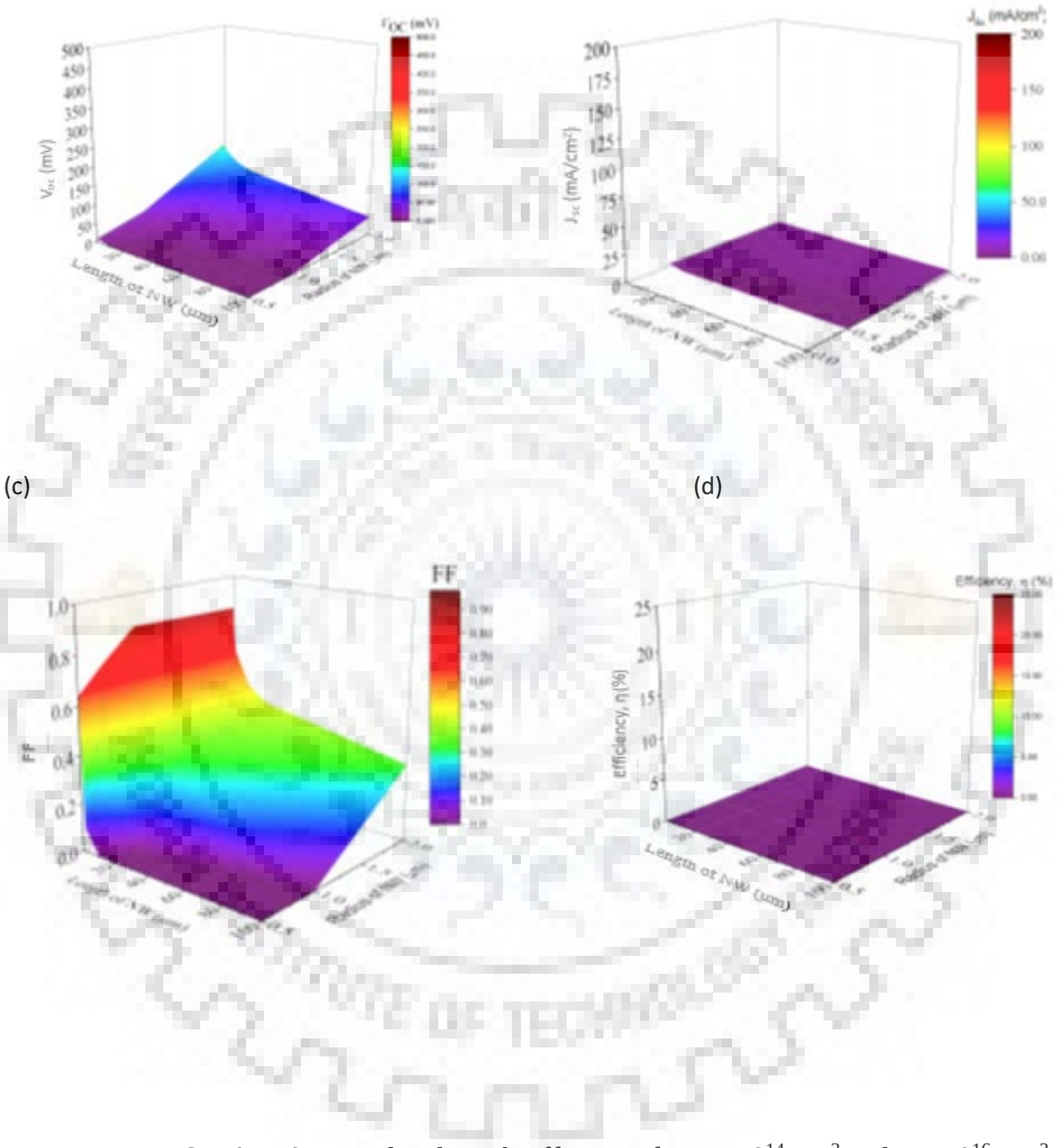

(c) (d)

Figure 4.6 MATLAB simulated graph Efficiency for $N_a=10^{14}$ cm^{-3} and $N_d=10^{16}$ cm^{-3}

(a)V_{oc}, (b) J_{sc} (c) FF (d)

(D) For $N_a=10^{14}$ cm^{-3} and $N_d=10^{17}$ cm^{-3}

(a) (b)

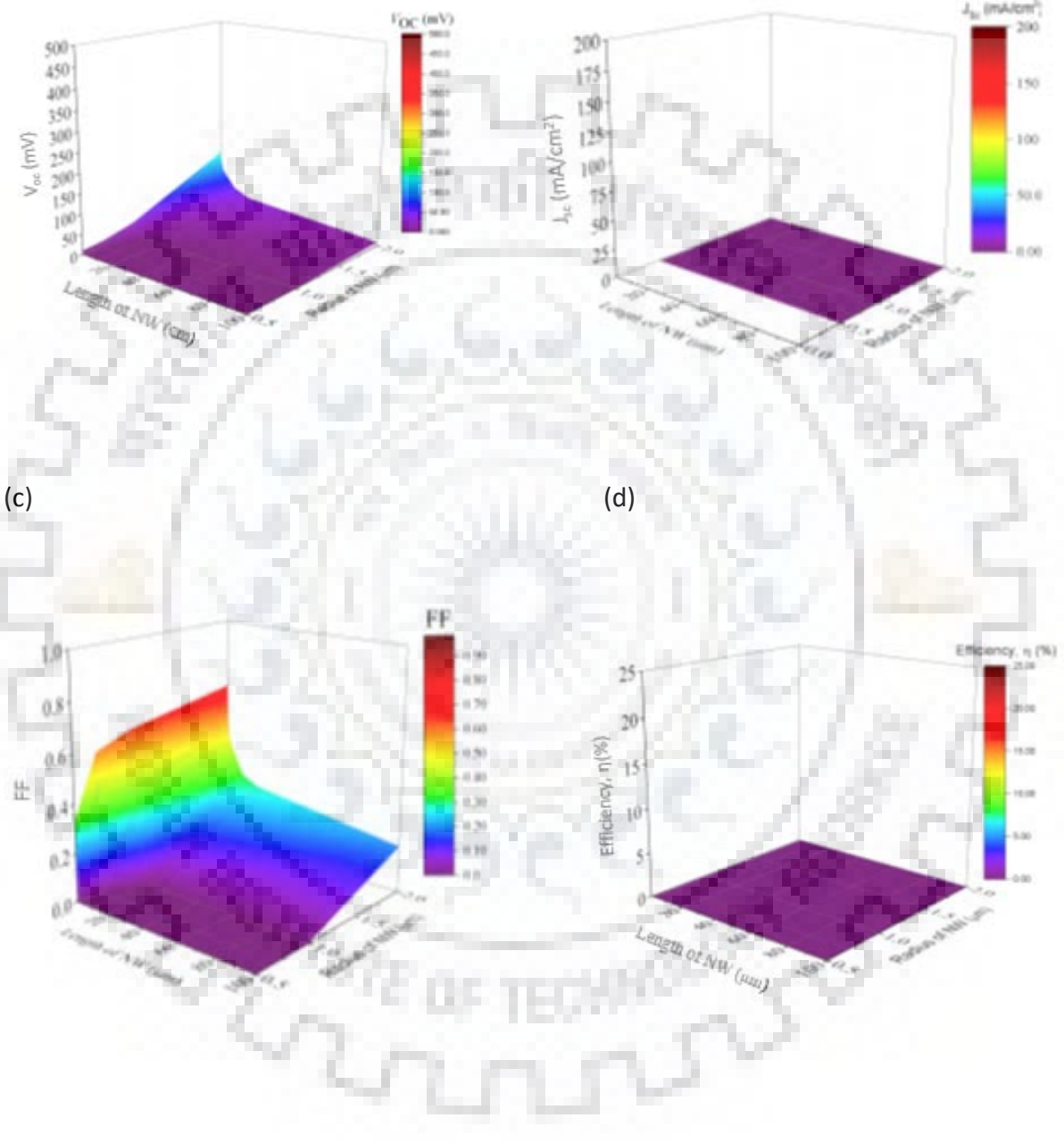

Figure 4.7 MATLAB simulated graph for $N_a=10^{14}$ cm^{-3} and $N_d=10^{17}$ cm^{-3}

(a)V_{oc}, (b) J_{sc} (c) FF (d) Efficiency

(E) For $N_a=N_d = 10^{15}$ cm^{-3}

(a) (b)

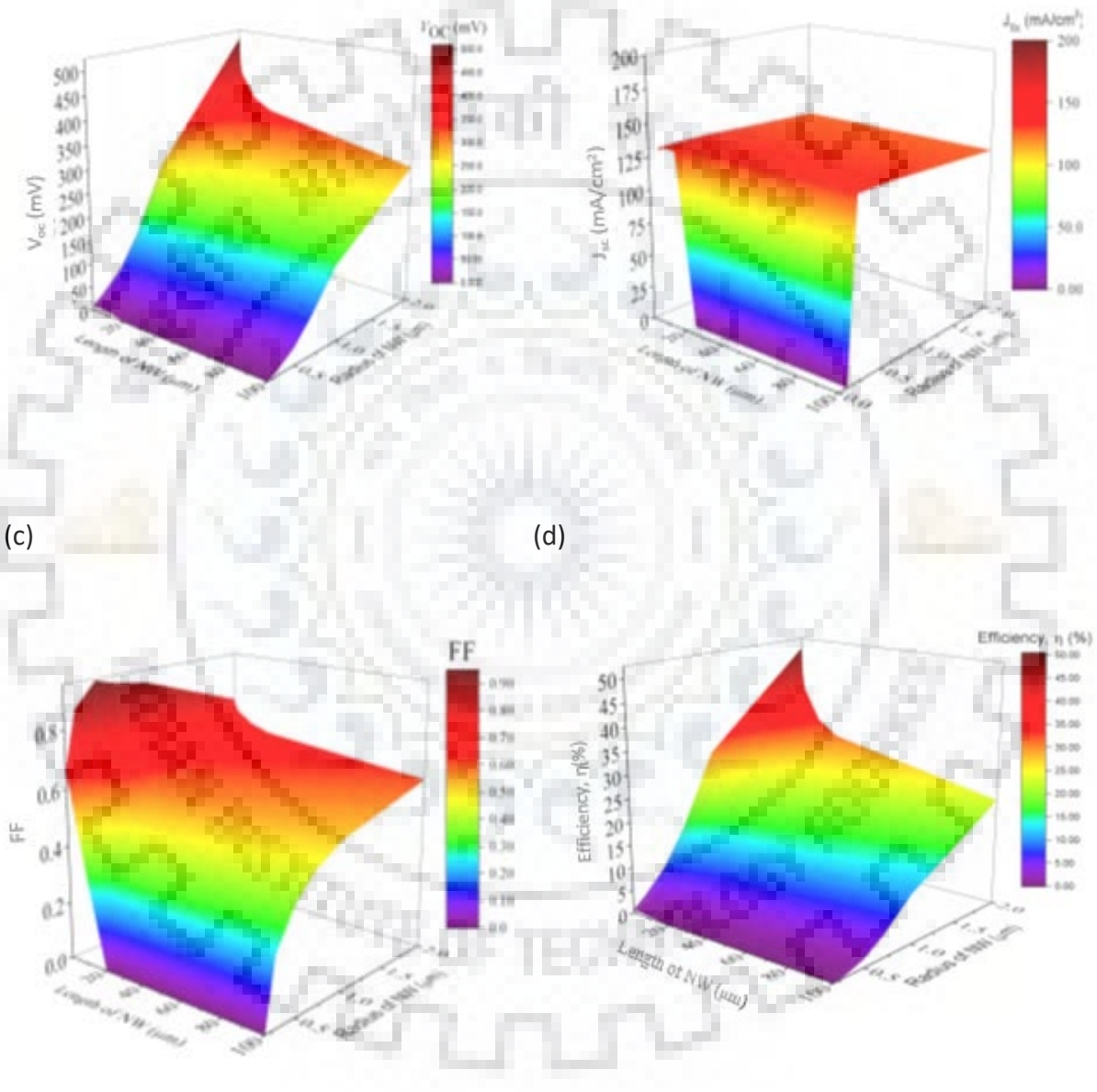

(c) (d)

Figure 4.8. MATLAB Simulated graph for $Na=N_d = 10^{15}$ cm^{-3}

(a)V_{oc}, (b) J_{sc} (c) FF (d) Efficiency

(F) For $N_a=N_d = 10^{16}$ cm^{-3}

(a) (b)

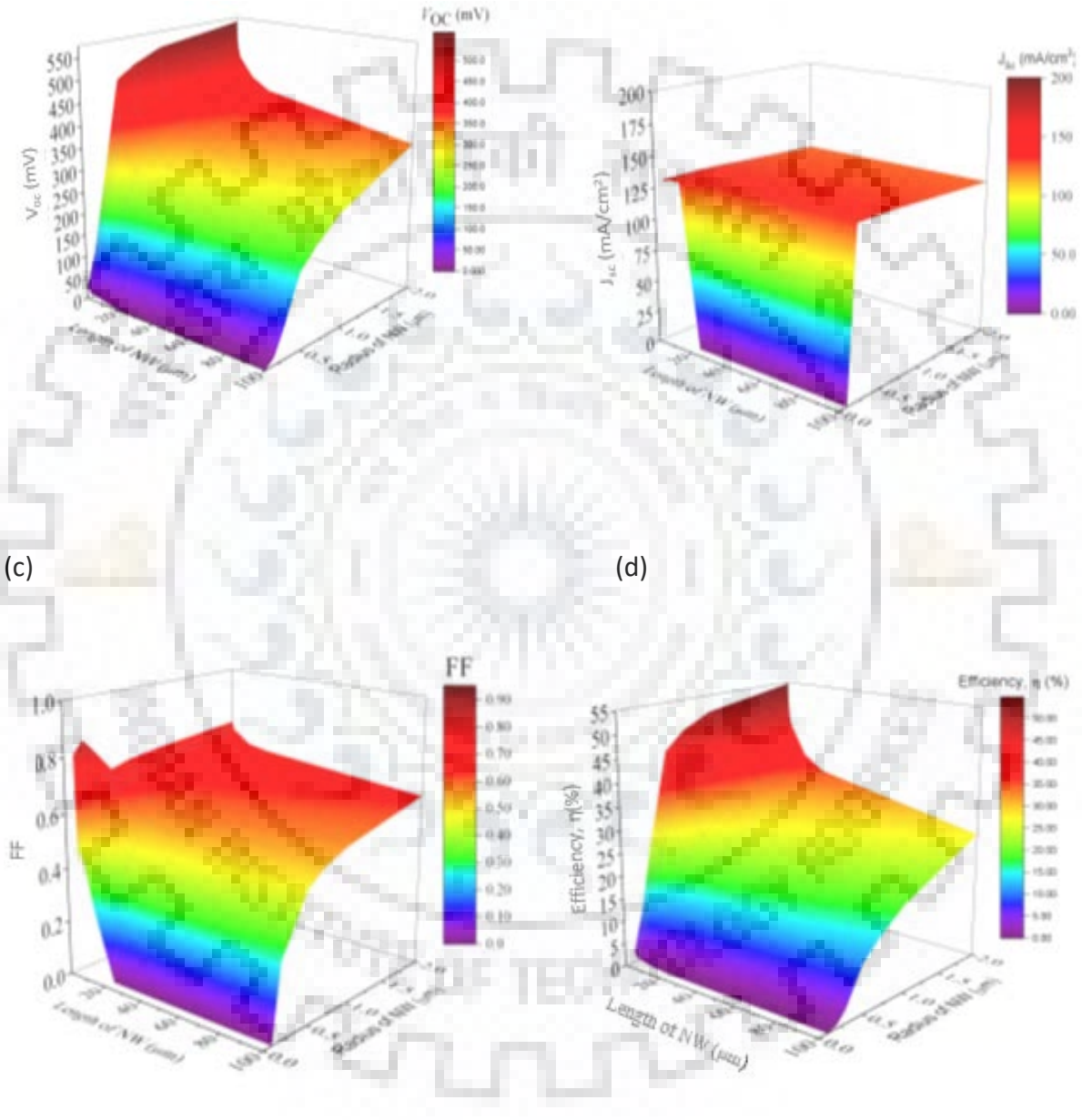

(c) (d)

Figure 4.9. MATLAB simulated graph for $Na=N_d = 10^{16}$ cm^{-3}

(a)V_{oc}, (b) J_{sc} (c) FF (d) Efficiency

(G) For $N_a=N_d = 10^{17}$ cm^{-3}

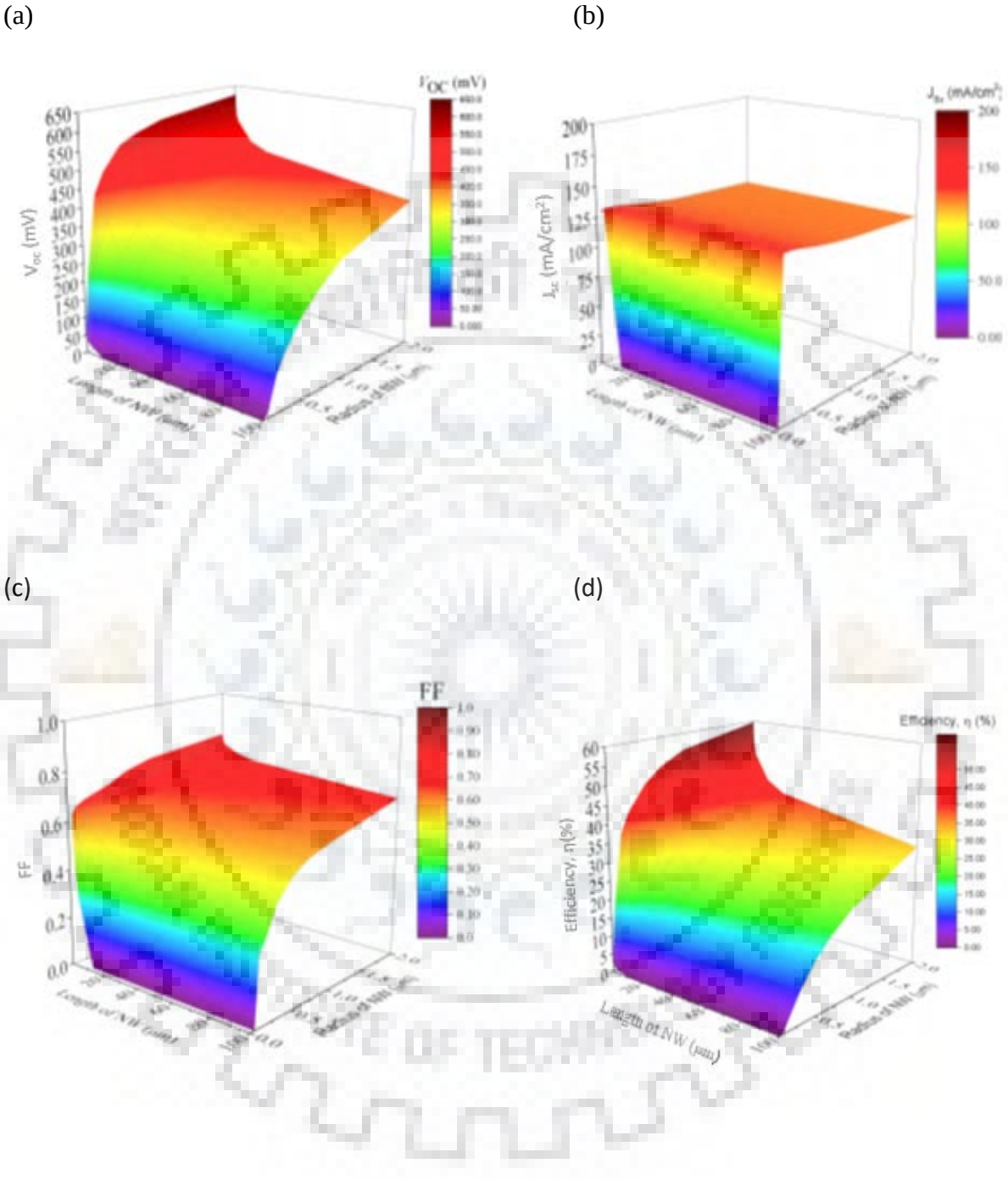

Figure 4.10. MATLAB simulated graph for $Na=N_d = 10^{17}$ cm^{-3}

(a)V_{oc}, (b) J_{sc} (c) FF (d) Efficiency

4.4 Discussion

As it earlier shown that for the same doping concentration the width of depletion region in core and shall will different, hence for the thin wire the doping concentration should be high so as to avoid the core fully depleted. Here, two regimes were treated

1. The trap density in the quasineutral region was assumed to be independent of the trap density in the depletion region , with the trap density in the depletion region set at low level such that depletion region trap had negligible effect on the cell performance
2. The trap density was assumed constant through the material, and thus the minority carrier lifetime in the quasineutral region and in the depletion region were identical. (it is more realistic)

The lifetimes in the depletion region is given by:

$$\tau_{n0} = \frac{1}{\sigma_n N_r v_{th}} \tag{4.35}$$

$$\tau_{p0} = \frac{1}{\sigma_p N_r v_{th}} \tag{4.36}$$

Where σ_n and σ_p are the cross section for the electron and hole capture, respectively, N_r is the density of recombination centers, and v_{th} is the thermal velocity.

In case (2), the high doping levels implies that

$$\tau_n \approx \tau_{n0} \tag{4.37}$$

$$\tau_p \approx \tau_{p0} \tag{4.38}$$

So that $\tau_n = \tau_p = \tau_{n0} = \tau_{p0}$ where τ_n and τ_p is the lifetime of minority carriers in p-type and in n-type quasineutral region respectively.

In case (1) quasineutral region recombination always being the dominant recombination mechanism while in case (2) quasineutral region recombination dominated for the $\tau_n \geq 40\ ns$, with depletion region recombination dominating for the shorter lifetimes.

It is clear from the above graph that J_{sc} increase with the increasing wire length, plateauing when the length of the wire become much greater that optical thickness of the material. Also J_{sc} was essential independent of the wire radius, provided that the radius was less than L_n. the

value of J_{sc} decreases abruptly for the R> L_n was essentially independent of the trap density in the depletion region.

The open circuit voltage V_{oc} decreases with the increasing wire length, and increases with increasing wire radius. The extent to which V_{oc} decreased with increasing with length depended strongly on the trap density in the depletion region, as the trap density became high in the depletion region, the V_{oc} declined steeply. The trap density in the quasineutral region, on the other hand had relatively less effect on V_{oc}.

Chapter 5

Methodology and the Experimental Result

5.1 Methodology

Nanowire can be grown on silicon wafer with metal assistant chemical etching in which the metal particle dissolve in solution act as a catalyst and when it comes with the contact to silicon wafer redox reaction takes place and metal particle bore into the silicon and create nanowire. Length of the nanowire can be controlled with time but the diameter controlling is not easy.

So, here we have shown that the diameter can be controlled by growing a self-assembly layer of nano particle which act a mask layer and guide to define the size of diameter.

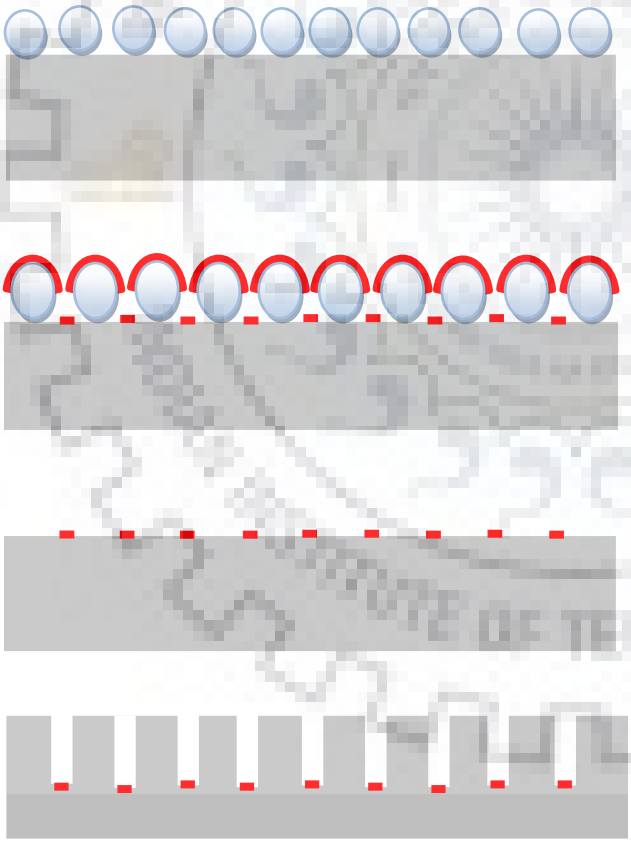

(a) 2-D non closed packed nanoparticle mask layer

(b) Metal catalyst deposited over it

(c) Lift of masking layer

(d) Nanowire after etching

Figure 5.1 Schematic illustration for fabricating Silicon nanowire

For preparing the solar cell absorber layer three step were used:

- Preparation of controlled size nanoparticle
- Self-assembled layer of nanoparticle by dip coating
- Preparation of nanowire by chemical etching method

5.1.1 Preparation of controlled size nanoparticle

Complete experiment were performed at room temperature without using any sophisticated instrument. Chemical and apparatus used are as follow[32]:

- TEOS (Tetraethylorthosilicate)
- Ammonium hydroxide
- Ethanol
- DI water
- Magnetic stirrer

Method:-

Preparation of nanoparticle require 8 to 10 hour with following required step:

Step 1:- First of all the required quantity of ethanol and ammonium hydroxide were taken in beaker and put it on the magnetic stirrer at room temperature. Speed of the stirrer should be between 250rpm to 300rpm.

Step 2:- After 10 min the DI water of required amount added while stirring and leave it for another 10 to 15 min on the stirrer

Step 3:- later the required quantity of TEOS were added immediately while stirring and after 10 min the color of solution changes. This complete reaction required time at least 8 to 10 hour. After the completion of reaction no change in turbidity is observed.

Step 4:- After the completion of reaction put the solution aside for another 48 to 72 hour to settle down the nanoparticle. After the nanoparticle get settle down remove the rest of solution and keep the precipitated white substance in the oven at 70^0C to dry.

The size of the nanoparticle can be estimated by the following expression. Which has been developed to fit the experimental observation[33]

$$d = A[H_2O]^2 exp\left(-B[H_2O]^{1/2}\right) \quad (5.1)$$

Where

$$A = [TEOS]^{1/2}(82 - 151[NH_3] + 1200[NH_3]^2 - 366[NH_3]^3) \quad (5.2)$$

$$B = 1.05 + 0.523[NH_3] - 0.128[NH_3]^3 \quad (5.3)$$

Above result were simulated on MATLAB (code in appendix) for various range of concentration and result are as follow:

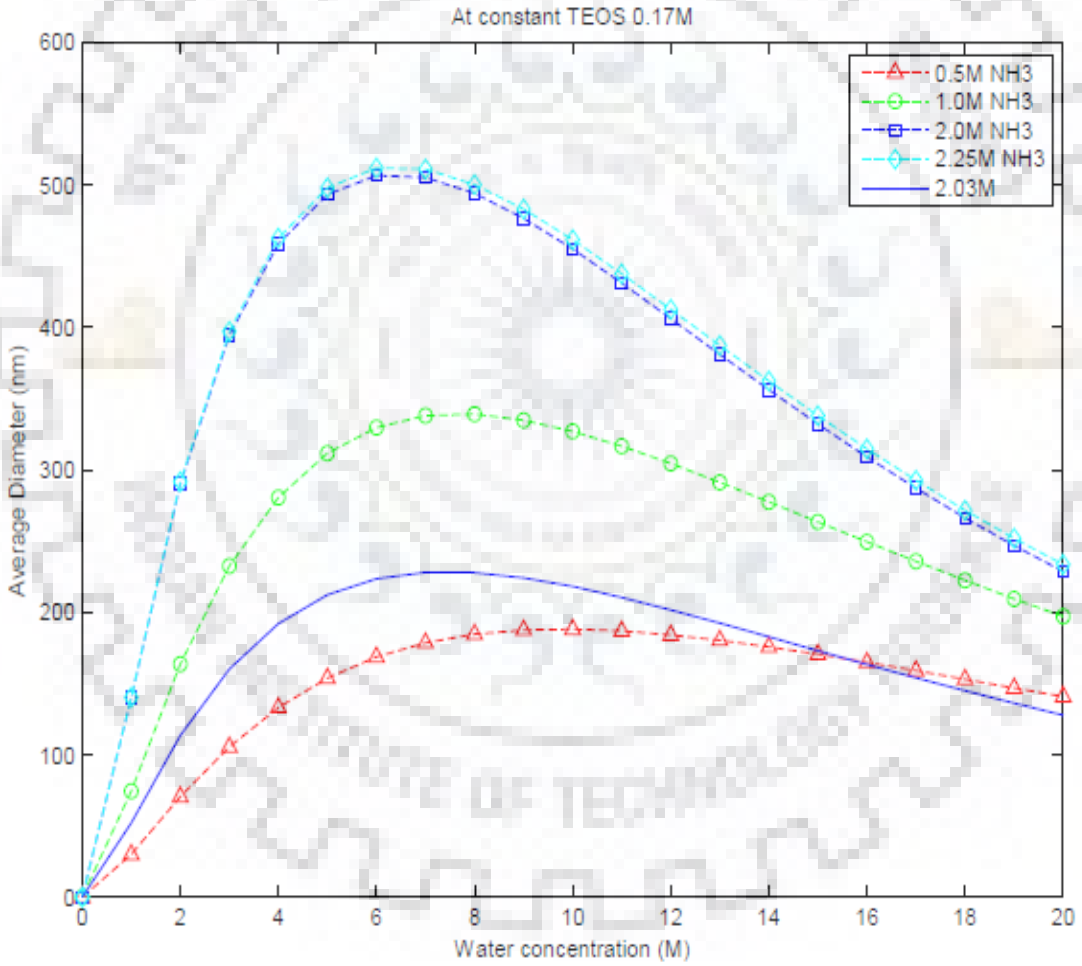

Figure 5.2 Variation in diameter of nanoparticle at constant TEOS 0.17M

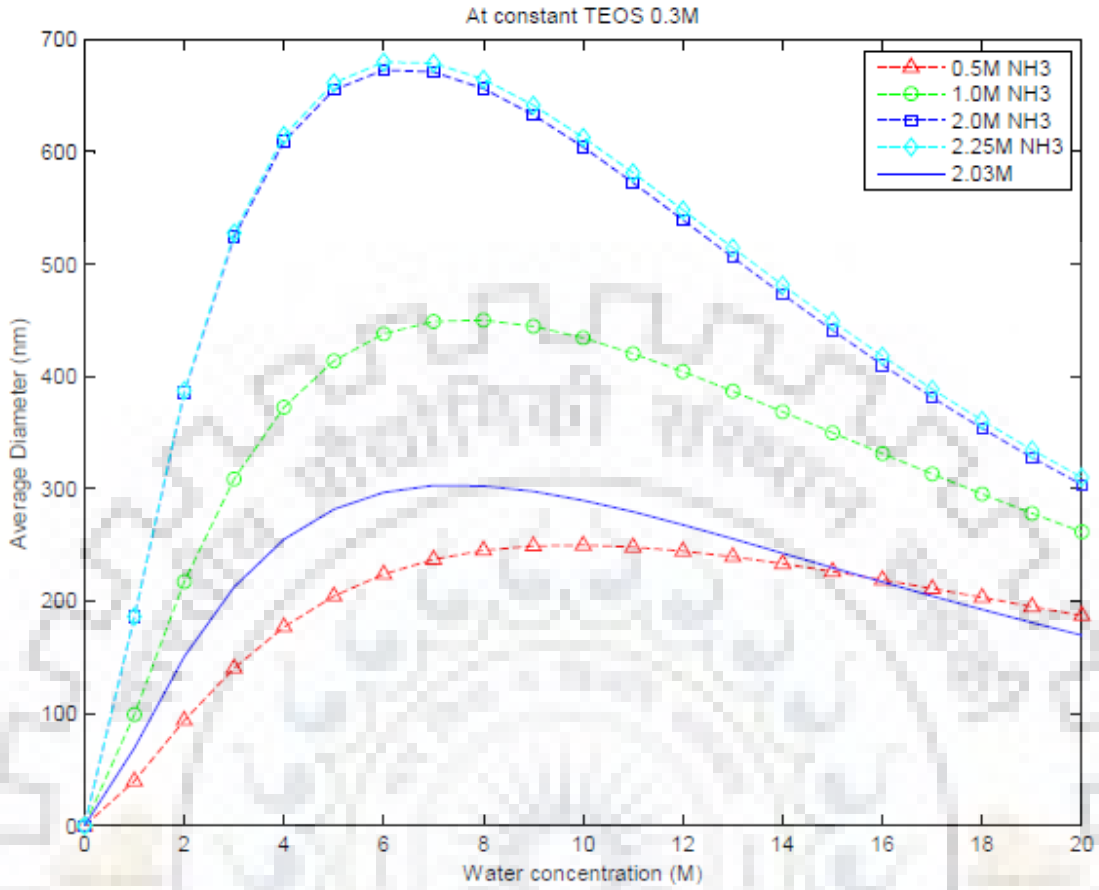

Figure 5.3 Variation in diameter of nanoparticle at constant TEOS 0.3M

5.1.2 Self-assembled layer of nanoparticle by dip coating

Monodispersed plain nanospheres of diameter 300nm and 500nm were prepared as the method given above. Than the silicon substrate were cleaned and immersed in the piranha solution containing 30% H_2O_2 and 70% H_2SO_4 in the ration of 1:4 for 2 to 3 hour than the sample were placed in $NH_4OH:H_2O_2:H_2O$ (1:1:5) at 80°C for 30min to make substrate hydrophilic[34].

Formation of monolayers*:* SAMs (self-assembled monolayers)[35],[36] of the nano particle were obtained by dipping silicon substrate into a well dispersed nanosphere suspension. Before dipping, the suspension was dispersed in an ultrasonic bath or with magnetic stirrer. During the coating the substrate was vertically dipped into the suspension for the few minute

and withdrawn at a programmed speed. The wet coating adhering to substrate was subsequently dried on hot plate magnetic stirrer. The coating parameter were:

- Concentration of the suspension 2-5 wt. %
- Withdrawal speed 1.4 – 2.5 mm/sec
- Immersion time 4 min
- Type of solvent (ethanol and water in 3:1 ratio)
- All dip coating performed at room temperature

Result and Discussion:-

Earlier dip coating were performed manually as a result which did not give the uniform monolayer. Partially dispersed monolayer and partially double layer were obtained as shown in fig.

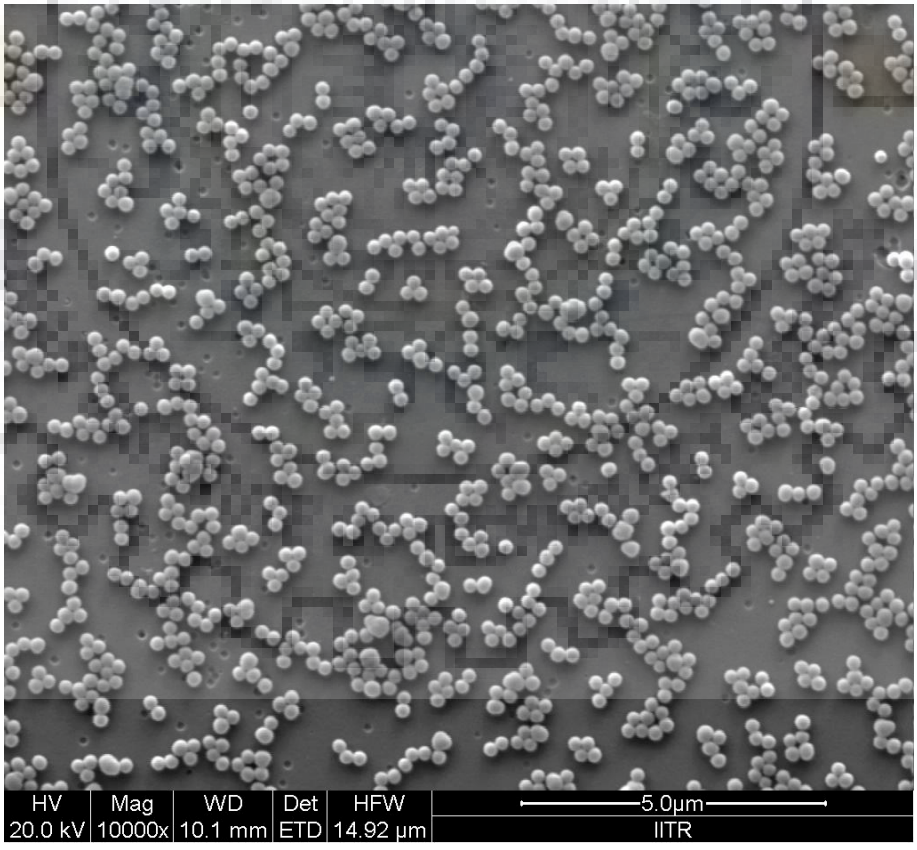

Figure 5.4 300 nm self-assembled dispersed monolayer

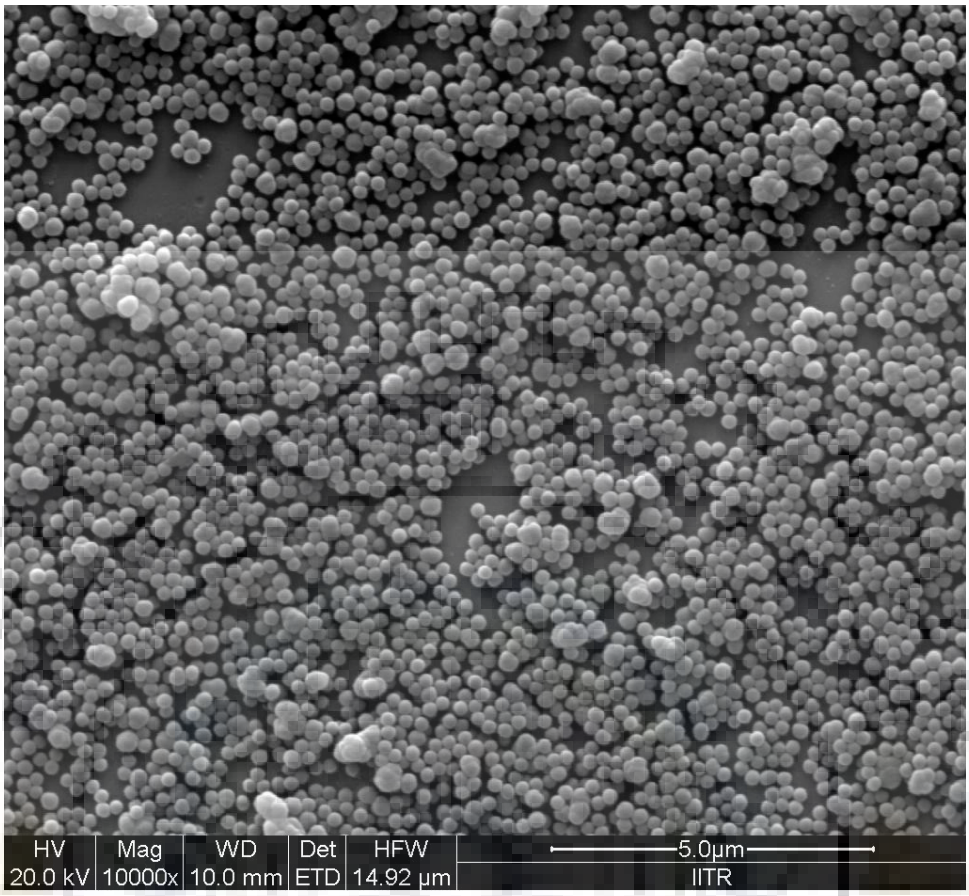

Figure 5.5 300nm self-assembled double layer

It should be noted that hexagonal closed packed structure is not formed everywhere over the substrate. A small area of multilayers and accumulation of nanosphere and sub monolayers with non-connected stipes and loosely packed islands can be observed at the bottom of the substrate (Fig. 5.7a) and sub monolayers with short range ordering and loosely packed islands are visible at the top of the substrate (Fig 5.7b) . This is attributed to interaction of all the factors: evaporation, capillary Particle –particle interaction, particle substrate interaction, concentration gradient in the suspension etc.

(a) (b)

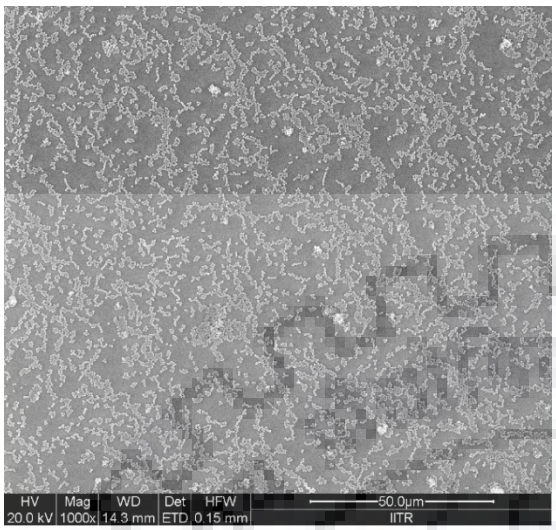

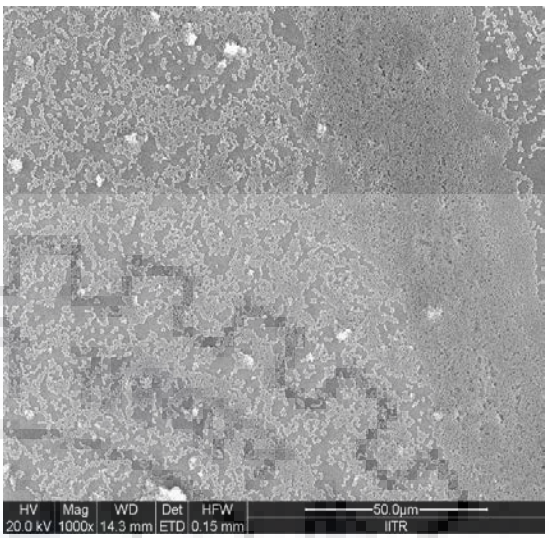

Figure 5.6a FESEM at the bottom of sample Figure 5.6b FESEM image at the top of sample

But under controlled speed by dip coater, proper humidity and balanced ration of water and ethanol well-ordered monolayer structure with good uniformity can be obtain as shown in fig. 5.7a and fig. 5.7b

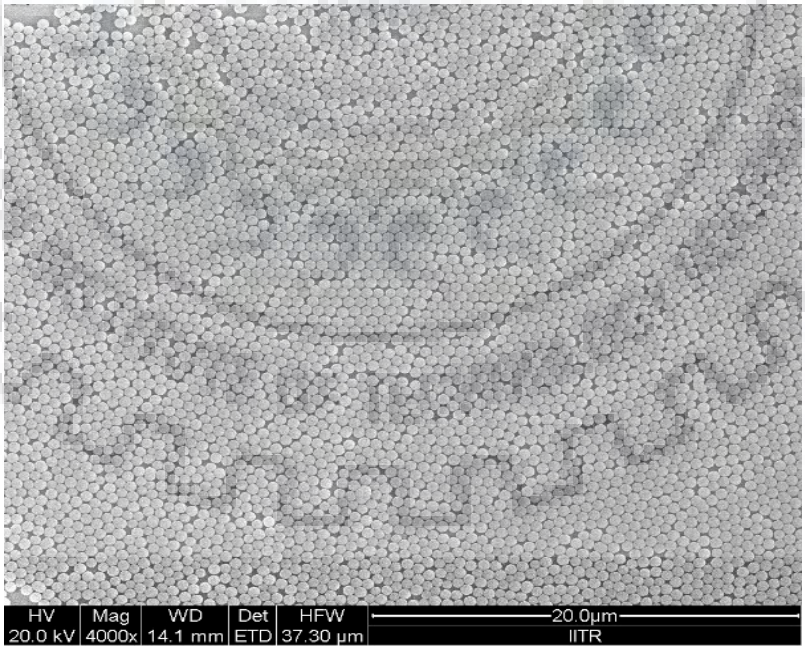

Figure 5.7a SAM layer at low resolution

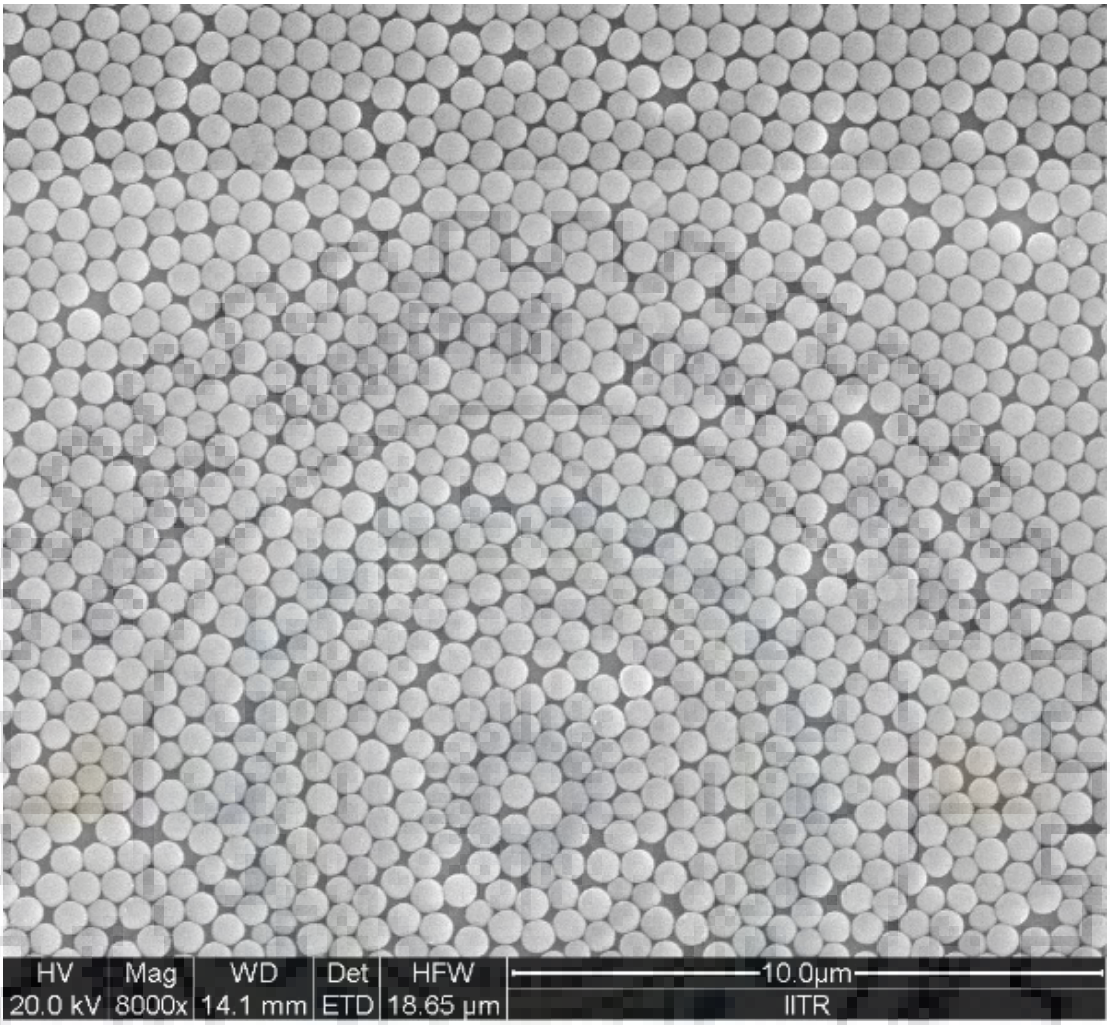

Figure 5.7b SAM layer at high resolution

Fig. 5.8 illustrate the process of dip coating, driven by the convective flux generated by the evaporation of the solvent in the meniscus region and the capillary forces. The particle size and density influence the balance among various elements. Successive particle arrays are expected to form continuously as the particle flux fills up the meniscus. The attraction by the lateral capillary forces leads to dense hexagonal packing. At the same time, the upward flux of particles undergoes particle- particle interaction and particle – substrate interaction

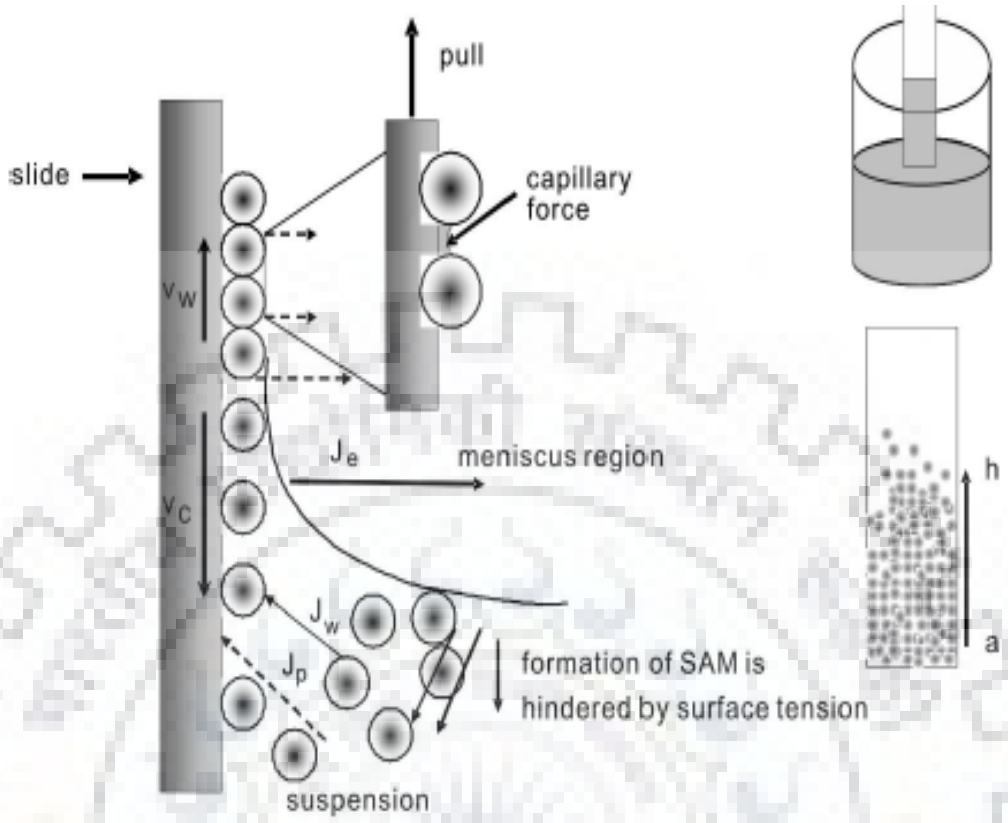

Figure 5.8 Scheme of the dip coating mechanism, where V_w-substrate withdrawal rate, V_c-monolayer growth rate, J_e- evaporation flux of solvent,J_w, J_p- entering fluxes of particle and solvent respectively[35]

5.1.3 Preparation of nanowire by chemical etching method

After getting the SAM layer of desired particle size, a metal catalyst is deposited onto silicon surface through the colloidal AM layer so as to fill the interstitial space by metal. After deposition of metal catalyst onto SAM, the silicon sample were placed in ultra-sonication in water for 2-3 min to remove the nano particle.

FESEM image of pattern transfer on sample is shown in Fig.5.9.

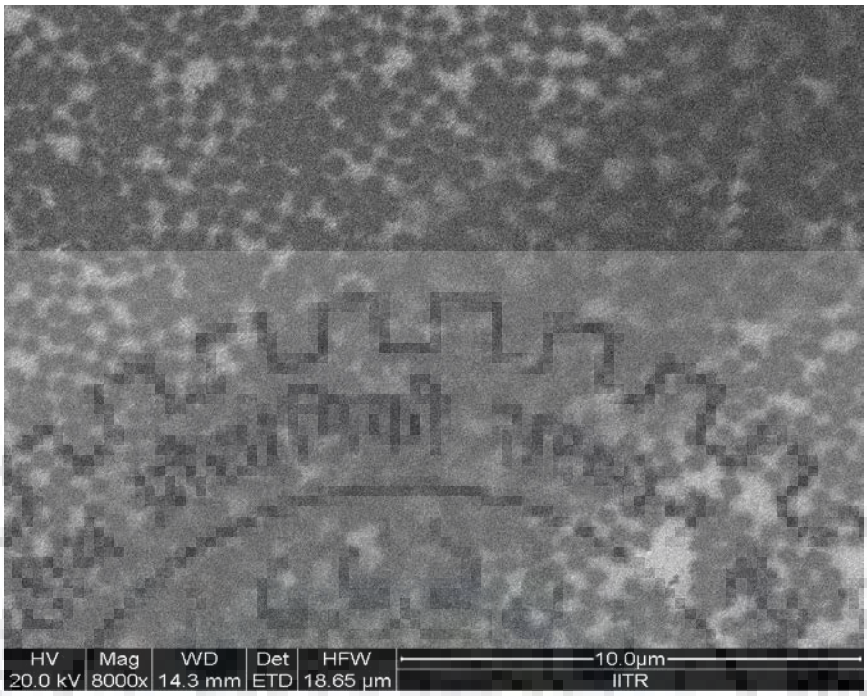

Figure 5.9a Transferred pattern after nano particle removal at low resolution

Figure 5.9b Transferred pattern after nano particle removal at high resolution

Finally, the sample were placed in oxidizing etchant solution for 10 min, and the pattern of metal particle was subsequently transferred to the silicon underneath.

By above said procedure two sample prepared, one with 300nm nano particle and other with 500 nm nano particle. Than FESEM images were taken at 45^{o} angle and vertical.

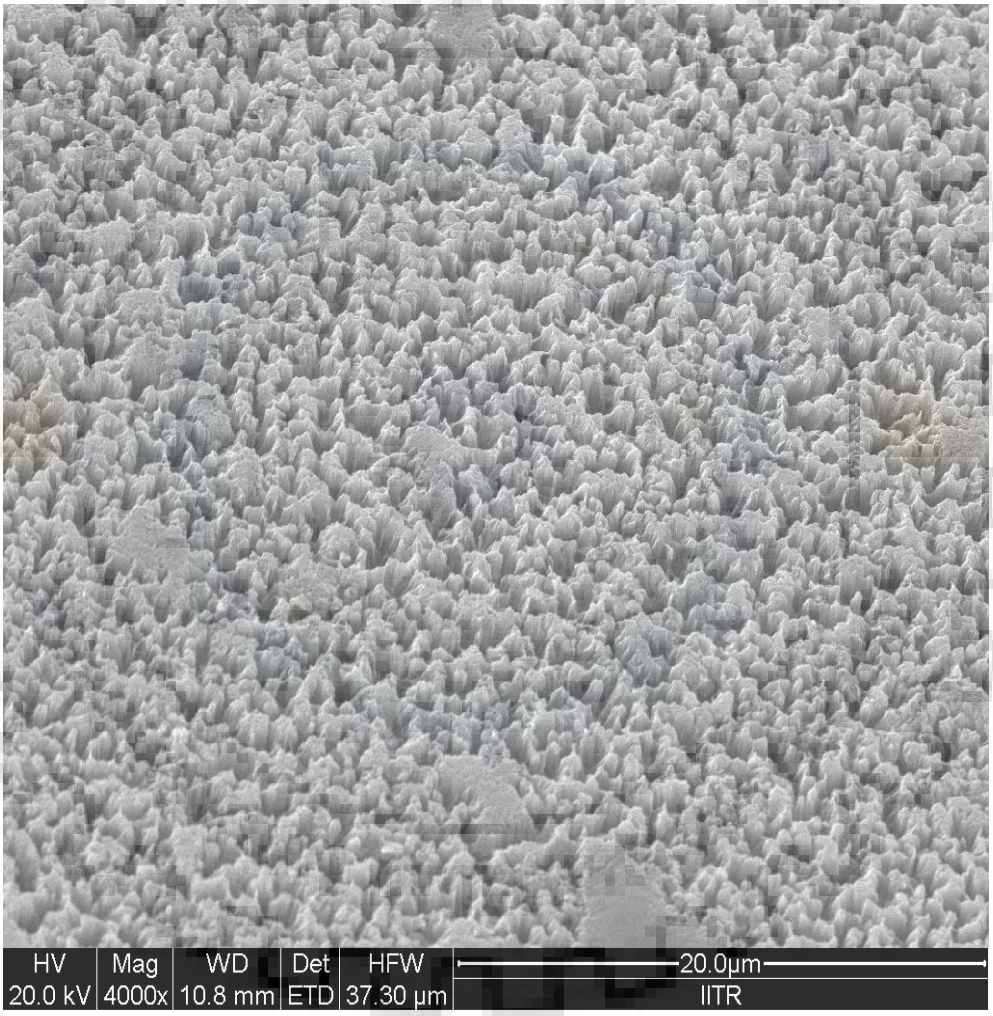

Figure 5.10a FESEM image SiNW at 45^{o} angle obtain by 300nm nano particle

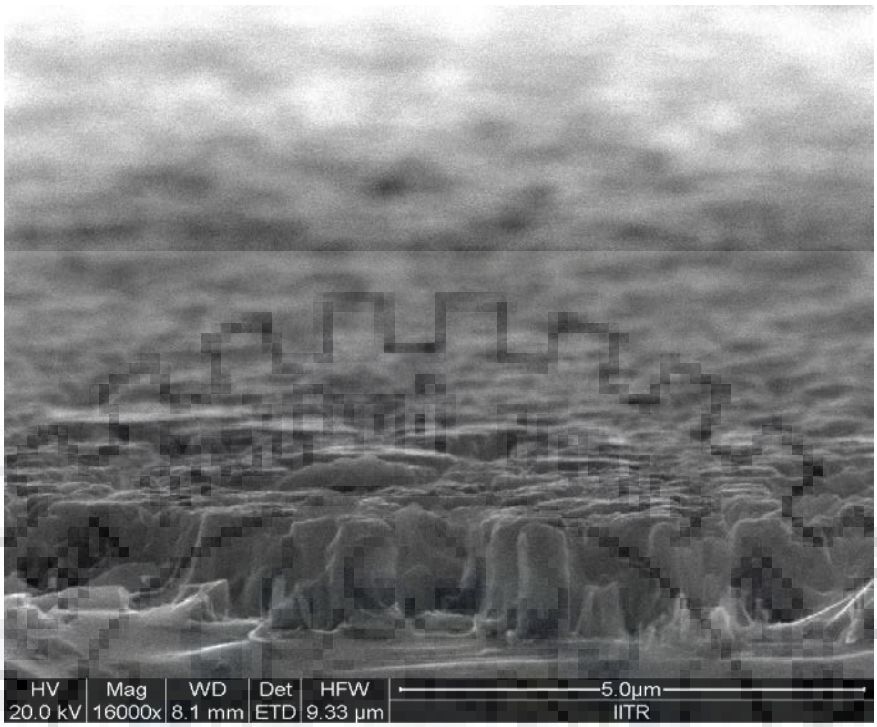

Figure 5.10b Vertical FESEM image SiNW obtain by 300nm nano particle

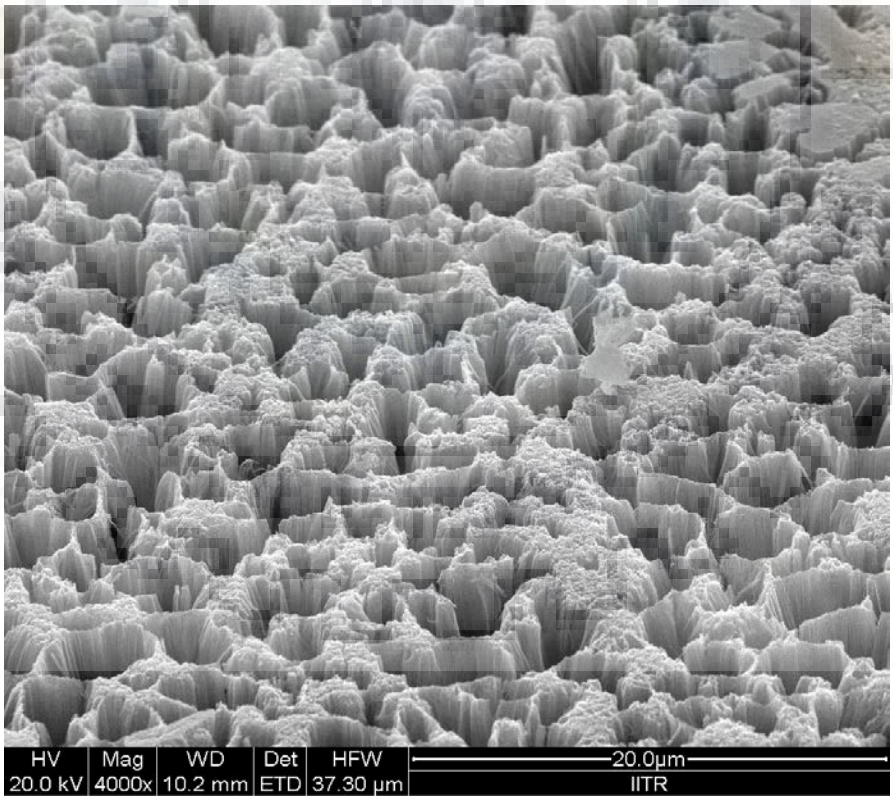

Figure 5.11a FESEM image SiNW at 45^{o} angle obtain by 500nm nano particle

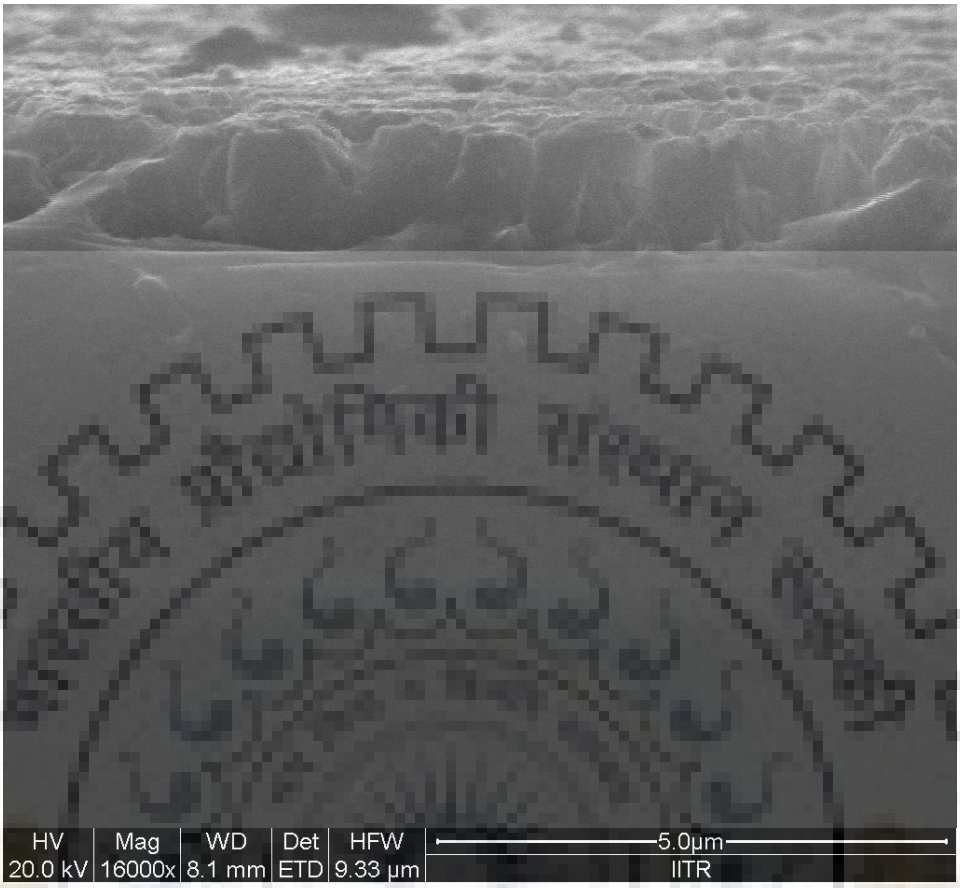

Figure 5.11b Vertical FESEM image SiNW obtain by 500nm nano particle

Analysis: - It is clearly observe from FESEM images that SiNWs of different diameter can be obtained by using the nano particle SAM which works as masking layer. In images, some flat portion is observer which arises due to handling while sample preparation for FESEM and at loading time. Wire seems to coagulate at the top of it is because larger length of nanowire get bend and stick to the neighboring wire, also surface of silicon substrate were made hydrophilic prior to the deposition SAM. By controlling the time and proper ration of chemical used for making etchant, controlled length and erected wire can be obtained

.

5.2 Ellipsometric Data

After preparing the diameter modulated nanowire, the ellipsometic data of prepared sample were compared with the ellipsometric result of bare silicon wafer. Ellipsometic results of above prepared data were done at the different angle 55º, 65º and 75º. Result obtained are as follow:

Ellipsometric data for bare cleaned silicon wafer (at 45º angle)

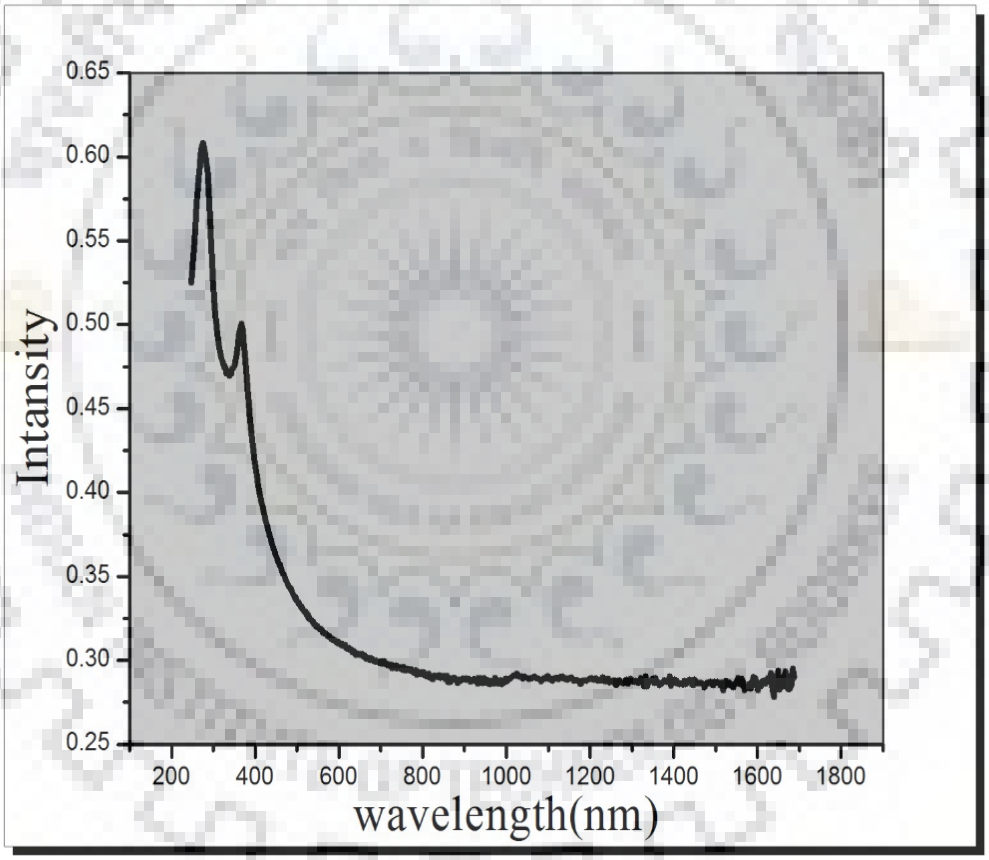

Figure 5.12 Reflectance of bare cleaned silicon wafer

Ellipsometric data for SiNWs prepared with 300nm nanoparticle

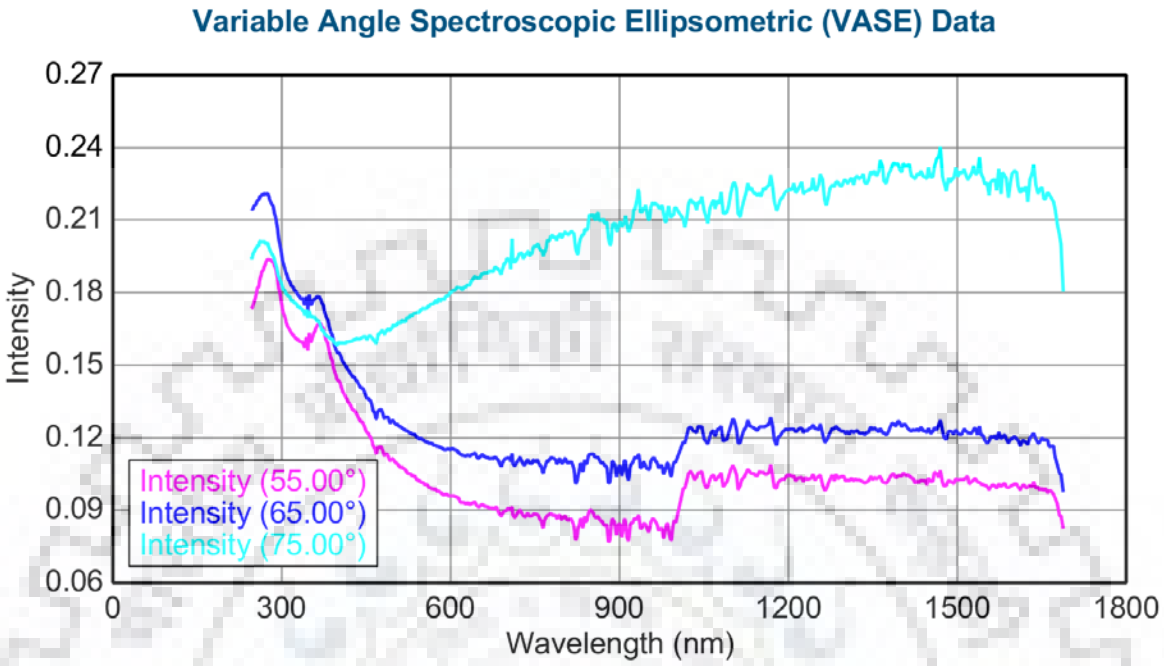

Figure 5.13 Reflectance of SiNW prepared with 300nm nano particle

Ellipsometric data for SiNWs prepared with 500nm nanoparticle

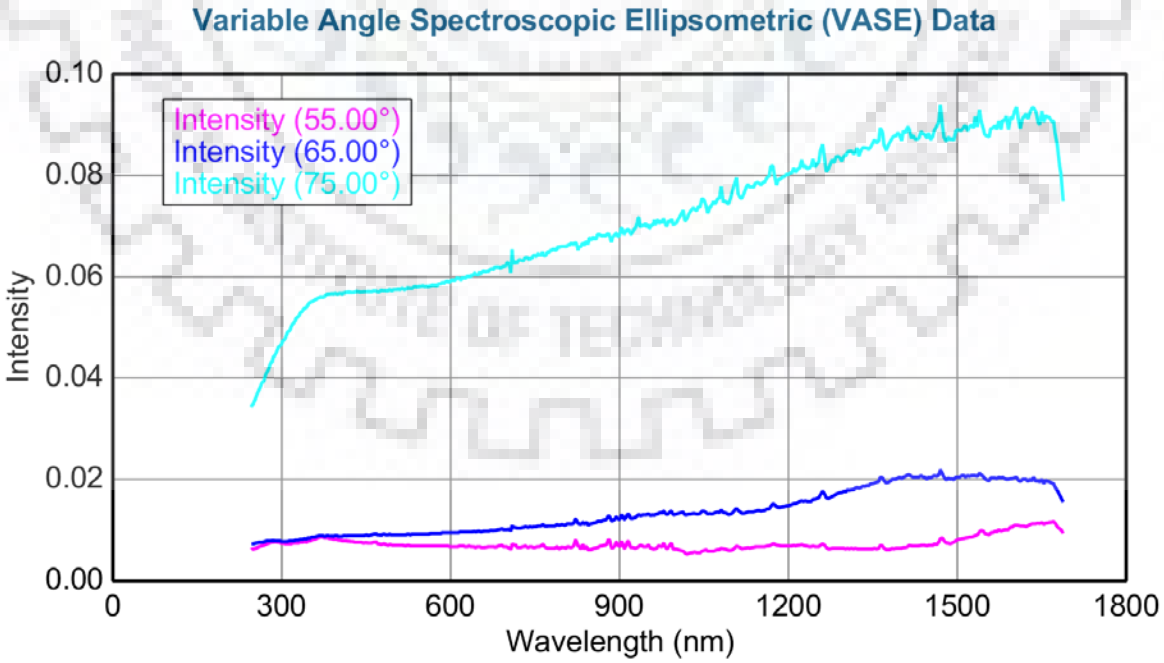

Figure 5.15 Reflectance of SiNW prepared with 500nm nano particle

Analysis: - If we compared SiNW obtained from 300nm nano particle with the bare cleaned silicon wafer than we see that reflectance is 12% for the visible region. This 12% reflectance is due to the pattern (see Fig. 5.9) in which assembled particle are touching, which increases effective surface area, as a result reflectance increases.

For the SiNW obtained for 500nm reflectance is less than 2% for the whole range of spectrum at 55^{o} angle and 65^{o} angle and increases up to 9% for the higher angle. Which is excellent reflectance for the solar cell.

Chapter 6

Conclusion and Future Work

In this thesis, we have explored that ability of radial p-n junction to enable PV device to have high conversion efficiency despite using low grade material. Here, we have shown the simulated data for various impurity, length and radius which can give high conversion efficiency if grown in controlled manner. It is also seen that depletion width is not same in core and shell for same impurity level. Hence, doping and diameter should be such that core is not completely depleted.

SiNW wire can be grown by metal assisted chemical etching method and can get NW of various length, but diameter cannot be controlled by this method. So, we have shown that how can we controlled the diameter of SiNW by chemical etching just by using the nano particle as masking layer, and this method can be used at room temperature without using sophisticated instrument.

In addition we have also studied the method to grow the nanoparticle of different size. For getting the different size of nano particle, we have simulated the experimentally obtain result which gives the estimation for the size of the nanoparticle. Later, we have shown that how this nanoparticle can be used to form SAM layer on silicon wafer which define the diameter of the SiNW.

The chemical etching method explained here can be used to obtain different surface morphology such as nano hole and inverted pyramid by proper adjusting the chemical ratio in etchant and by changing the nano particle surface morphology.

SiNW grown on silicon surface does not cover the complete area i.e. the fill factor (ratio of SiNW grown area to the total surface area) also plays an important role for getting the optimum conversion efficiency which is not studied here. Therefore, the future study should be address to optimize the fill factor and to fabricate solar cell by using the nanowire, inverted pyramid and nanohole.

Appendix A

MATLAB Simulation Code[27]

A.1 Radial p-n Junction Simulation

This is the simulation code for the radial p-n junction:-

```
clear all
format short g
warning off MATLAB:fzero:UndeterminedSyntax
warning off MATLAB:divideByZero
E = linspace(0,4,50);   %energy in ev
flux = linspace(0,4*10^17,50); % Flux vector in per cm^2 per sec per ev
alpha = linspace (10,10^6,50);    % range of absorption coefficient in per cm
n=length(E)-1;
dE=(E(2:(n+1))-E(1:n));
alpha2=alpha(2:(n+1));
alpha1=alpha2; % alpha1 and alpha2 are the absorption coefficients of the n and p-type
materials, respectively
gammaA=flux(2:(n+1));
gammaC=gammaA; % gammaA and gammaA are the photon fluxes incident on the top of
…the n- and p-type quasineutral regions, respectively
matrix=[];
lengths=[1e-5,3e-5,5e-5,7e-5,1e-4,1.5e-4,2e-4,1e-3,2e-3,1e-2]; % lengths is a vector
containing the various cell thicknesses that will be considered, in cm
thing=length(lengths);
%dope=[1,10,1e2,1e3,1e4,1e5,1e6,1e7,1e8]*5e12;
%muele=[1500,1500,1500,1500,1000,400,150,100,100];
%muhol=[500,500,500,400,300,150,60,50,50]; %these lines indicate the maximum
...electron and hole mobilities possible in Si at various doping levels,
%max Na = [>1e20, >1e20, 9e19, 4e19, 2e19, 9e18, 4e18, 2e18, 8e17, 3e17]
```

```
%vs Ln = [1e-5, 2e-5, 5e-5, 1e-4, 2e-4, 5e-4, 1e-3, 2e-3, 5e-3, 1e-2]
% => mun= [95, 95, 95, 100, 110, 130, 160, 195, 300, 540] %these lines
...indicate the maximum electron diffusion length possible in Si at various doping levels
%Define constants
q=1.60219e-19;
kB=1.3807e-23;
T=300;
%Silicon data
%Eg=1.12;
Nc=2.8e19;
Nv=1.04e19;
ni=1.4e10;
Na=1e15;
mun=270;
Nd=1e18;
mup=95;
Dn=kB*T/q*mun;
Dp=kB*T/q*mup;
Sn=1e5;
sigman=1e-15;
sigmap=sigman;
vth=1e7;
if  ni^2>=Na*Nd
   break
end
np0=ni^2/Na;
pn0=ni^2/Nd;
Vbi=kB*T/q*log(Na*Nd/ni^2);
epsilon0=8.85418e-14;
epsilonn=11.9*epsilon0; epsilonp=epsilonn; epsilons=epsilonn;
R=[1e-6,2e-6,5e-6,1e-5,2e-5,3e-5,5e-5,7e-5,1e-4,2e-4]; % R is a vector
```

```
...containing the various cell radii that will be considered, in cm
N=length(R);
count=1:N;
for thingee=1:thing
   L=lengths(thingee)*ones(1,N);
   aspectratio=L./R;
   V=linspace(0,95/100*Vbi); %the program assumes that Voc < 0.95 Vbi
   NN=length(V);
   x1=zeros(NN,N);
   x2=zeros(NN,N);
   x3=zeros(NN,N);
   x4=zeros(NN,N);
   J0A=zeros(NN,N);
   J0C=zeros(NN,N);
   J0=zeros(NN,N);
   JlAperE=zeros(n,N,NN);
   JlCperE=zeros(n,N,NN);
   JlA=zeros(NN,N);
   JlC=zeros(NN,N);
   Jl=zeros(NN,N);
   Jrdep=zeros(NN,N);
   JdepAperE=zeros(n,N,NN);
   JdepCperE=zeros(n,N,NN);
   JdepA=zeros(NN,N);
   JdepC=zeros(NN,N);
   Jgdep=zeros(NN,N);
   J=zeros(NN,N);
   bias=zeros(NN,N);
   VBI=zeros(NN,N);
   Voc=zeros(1,N);
   Jsc=zeros(1,N);
```

```
A1A=zeros(NN,N);
A1C=zeros(NN,N);
A2A=zeros(NN,N);
A2C=zeros(NN,N);
B1A=zeros(NN,N);
B2A=zeros(NN,N);
for i = 1:N
   disp(round(((thingee-1)/thing+i/(thing*N))*100)) %a counter, so that the user doesn't
…think the program has crashed
   for ii= 1:NN
      Ln=R(i); %setting radius = minority electron diffusion length
      Nr=Dn/(Ln^2*sigman*vth);
      taun0=1/(sigman*Nr*vth);
      taup0=1/(sigmap*Nr*vth);
      taun=taun0;taup=taup0;
      %taun0=1e-6; taup0=taun0; %activate this line to set the depletion
      ...region minority electron lifetime? n0 separately from the
      ...quasineutral region minority electron lifetime? n (similarly for holes)
      Lp=sqrt(taup*Dp);
      windowwidth=1e-6; %minimum emitter thickness, in cm
      bias(ii,i)=V(ii);

[x1(ii,i),x2(ii,i),x3(ii,i),x4(ii,i),VBI(ii,i)]=depletionregion(Nd,Na,R(i),epsilonp,epsilonn,ni,bi
as(ii,i),windowwidth);
      if bias(ii,i)>VBI(1,i)
         break
      end
      d1(ii,i)=x1(ii,i)+x2(ii,i);
      d2(ii,i)=x3(ii,i)+x4(ii,i);
      %define dimensionless variables
      beta1(ii,i)=R(i)/Lp;
```

```
beta2(ii,i)=(R(i)-x1(ii,i))/Lp;
beta3=alpha1*L(i);
beta4=Lp*Sn/Dp;
beta5(ii,i)=x4(ii,i)/Ln;
beta6=alpha2*L(i);
f1(ii,i)=besseli(1,beta1(ii,i))+beta4*besseli(0,beta1(ii,i));
f2(ii,i)=besselk(1,beta1(ii,i))-beta4*besselk(0,beta1(ii,i));
JlnperE(:,i,ii)=-2*q*gammaA*beta2(ii,i)/(beta1(ii,i))^2*...
   (-besseli(1,beta2(ii,i))*(f2(ii,i)+beta4*...
   besselk(0,beta2(ii,i)))+besselk(1,beta2(ii,i))*(f1(ii,i)-...
   beta4*besseli(0,beta2(ii,i))))/(f1(ii,i)*...
   besselk(0,beta2(ii,i))+f2(ii,i)*besseli(0,beta2(ii,i))).*(1-exp(-beta3)).*dE;
Jln(ii,i)=sum(JlnperE(:,i,ii));
J0n(ii,i)=2*L(i)*q*pn0/taup*beta2(ii,i)/(beta1(ii,i))^2*...
   (f2(ii,i)*besseli(1,beta2(ii,i))-f1(ii,i)*...
   besselk(1,beta2(ii,i)))/(f1(ii,i)*besselk(0,beta2(ii,i))+...
   f2(ii,i)*besseli(0,beta2(ii,i)));
JlpperE(:,i,ii)=2*q*gammaC*Ln^2/Lp^2*beta5(ii,i)/...
   (beta1(ii,i))^2*besseli(1,beta5(ii,i))/...
   besseli(0,beta5(ii,i)).*(1-exp(-beta6)).*dE;
Jlp(ii,i)=sum(JlpperE(:,i,ii));
Jlp(ii,i)=-Jlp(ii,i);
J0p(ii,i)=-2*L(i)*q*np0*Dn/Lp^2*beta5(ii,i)/(beta1(ii,i))^2*...
   besseli(1,beta5(ii,i))/besseli(0,beta5(ii,i));
JgdepnperE(:,i,ii)=-q*gammaA*((d2(ii,i)+x2(ii,i))^2-...
   (d2(ii,i))^2)/(R(i))^2.*(1-exp(-beta3)).*dE;
Jgdepn(ii,i)=sum(JgdepnperE(:,i,ii));
JgdeppperE(:,i,ii)=-q*gammaC*((d2(ii,i))^2-(x4(ii,i))^2)/...
   (R(i))^2.*(1-exp(-beta6)).*dE;
Jgdepp(ii,i)=sum(JgdeppperE(:,i,ii));
U(ii,i)=1/2*ni/sqrt(taun0*taup0)*2*sinh(q*bias(ii,i)/(2*kB*T));
```

```
        kappa(ii,i)=pi*kB*T/(q*(VBI(ii,i)-bias(ii,i)));
        r(ii,i)=x4(ii,i)+(log(Na/ni))/(log(Nd/ni)+log(Na/ni))*(x2(ii,i)+...
            x3(ii,i));
        r2(ii,i)=r(ii,i)+(x2(ii,i)+x3(ii,i))*1/2*kappa(ii,i);
        r1(ii,i)=r(ii,i)-(x2(ii,i)+x3(ii,i))*1/2*kappa(ii,i);

        Jrdep(ii,i)=-q*L(i)*U(ii,i)*(r2(ii,i)^2-r1(ii,i)^2)/(R(i))^2;
    end
end
Jgdep=Jgdepn+Jgdepn;
Jgdep=[Jgdep;zeros(NN-length(Jgdep),N)];
Jl=Jln+Jlp;
Jl=[Jl;zeros(NN-length(Jl),N)];
J0=J0n+J0p;
J0=[J0;zeros(NN-length(J0),N)];
J=(J0.*(exp(q*bias/(kB*T))-1)-Jl-Jgdep+Jrdep);
temp=[J(1,:);zeros(NN-1,N)];
J(bias==0)=0;
J=J+temp;
P=J.*bias;
P(P<0)=0;
[maxP,posn]=max(P);
eff=maxP/(.1)*100;
Jsc=J(1,:);
b=sum(J>0);
for j=1:N;
    if b(j)~=0
        if b(j)==100
            Voc(j)=0;
        elseif bias(b(j)+1,j)==0
            Voc(j)=0;
```

```
        else
            Voc(j)=(bias(b(j),j)+bias(b(j)+1,j))/2;
        end
    else
        Voc(j)=0;
    end
end
ff=maxP./(Voc.*Jsc);

arshort=aspectratio(ff<0.9999&ff>0)
Lshort=L(ff<0.9999&ff>0);
Rshort=R(ff<0.9999&ff>0);
Vocshort=Voc(ff<0.9999&ff>0);
Jscshort=Jsc(ff<0.9999&ff>0);
ffshort=ff(ff<0.9999&ff>0);
effshort=eff(ff<0.9999&ff>0);
%disp(' Aspect Ratio L (cm) R (cm) Jsc (A/cm^2) Voc (V) ff Efficiency(%)')
%disp([aspectratio', L',R',Jsc', Voc', ff', eff'])
matrix=[matrix; arshort', Lshort',Rshort',effshort', Jscshort',Vocshort', ffshort'];
end
t1=num2str(Lp,4);
t2=num2str(Ln,4);
t3=num2str(Sn,4);
t6=num2str(mup,4);
t7=num2str(mun,4);
t8=num2str(Na,4);
t9=num2str(Nd,4);
t10=num2str(windowwidth,4);
t11=num2str(taun0,4);
t12=num2str(taup0,4);
```

```
name=sprintf('Radial Silicon matrix Ln=%s, Lp=%s, Sn=%s, taun0=%s, taup0=%s, Na=%s,
Nd=%s, window width=%s.txt', t2,t1,t3,t11,t12,t8,t9,t10);
save(name,'matrix','-ASCII','-TABS')
Rmin=min(matrix(:,3));
Rmax=max(matrix(:,3));
R=R((R>=Rmin)&(R<=Rmax));
nR=length(R);
Lmin=min(matrix(:,2));
Lmax=max(matrix(:,2));
L=lengths((lengths>=Lmin)&(lengths<=Lmax));
nL=length(L);
index=cumsum(ones(1,nR));
for i = 1:nL
   temp=matrix(matrix(:,2)==L(i),4);
   temp=temp';
   tempJsc=matrix(matrix(:,2)==L(i),5);
   tempJsc=tempJsc';
   tempVoc=matrix(matrix(:,2)==L(i),6);
   tempVoc=tempVoc';
   tempff=matrix(matrix(:,2)==L(i),7);
   tempff=tempff';
   posR=(min(matrix(matrix(:,2)==L(i),3))==R)*index';
   matrix2(i,:)=[zeros(1,posR-1),temp,zeros(1,nR-length(temp)-posR+1)];
   matrixJsc(i,:)=[zeros(1,posR-1),tempJsc,zeros(1,nR-length(tempJsc)-posR+1)];
   matrixVoc(i,:)=[zeros(1,posR-1),tempVoc,zeros(1,nR-length(tempVoc)-posR+1)];
   matrixff(i,:)=[zeros(1,posR-1),tempff,zeros(1,nR-length(tempff)-posR+1)];
end
matrix2=[L',matrix2];
matrix2=[0,R;matrix2];
matrix2(:,2);
matrixJsc=[L',matrixJsc];
```

```
matrixJsc=[0,R;matrixJsc];
matrixVoc=[L',matrixVoc];
matrixVoc=[0,R;matrixVoc];
matrixff=[L',matrixff];
matrixff=[0,R;matrixff];

matrix(:,4:6)

maxeff=num2str(max(max(matrix2)),3);
[junk, row]=max(matrix2);
[junk, column]=max(max(matrix2));
row=row(column);
name2=sprintf('Radial Silicon Eff Ln=%s, Lp=%s, Sn=%s, taun0=%s,taup0=%s, Na=%s,
Nd=%s, window width=%s, maxeff=%s.txt',t2,t1,t3,t11,t12,t8,t9,t10,maxeff);
name3=sprintf('Radial Silicon Jsc Ln=%s, Lp=%s, Sn=%s, taun0=%s,taup0=%s, Na=%s,
Nd=%s, window width=%s, maxeff=%s.txt',t2,t1,t3,t11,t12,t8,t9,t10,maxeff);
name4=sprintf('Radial Silicon Voc Ln=%s, Lp=%s, Sn=%s, taun0=%s,taup0=%s, Na=%s,
Nd=%s, window width=%s, maxeff=%s.txt',t2,t1,t3,t11,t12,t8,t9,t10,maxeff);
name5=sprintf('Radial Silicon ff Ln=%s, Lp=%s, Sn=%s, taun0=%s,taup0=%s, Na=%s,
Nd=%s, window width=%s, maxeff=%s.txt',t2,t1,t3,t11,t12,t8,t9,t10,maxeff);
save(name2,'matrix2','-ASCII','-TABS')
save(name3,'matrixJsc','-ASCII','-TABS')
save(name4,'matrixVoc','-ASCII','-TABS')
save(name5,'matrixff','-ASCII','-TABS')
figure(1)
surf(log10(R),log10(L),matrix2(2:(nL+1),2:(nR+1)))
xlabel('log_{10}(R) (log_{10}(cm))')
ylabel('log_{10}(L) (log_{10}(cm))')
zlabel('Efficiency (%)')
name2a=sprintf('Radial cell Eff. with Ln=%s, Na=%s, Nd=%s, Sn=%s,maxEff=%s',
t2,t8,t9,t3, maxeff);
```

```
title(name2a)

figure(2)
surf(log10(R),log10(L),matrixJsc(2:(nL+1),2:(nR+1)))
xlabel('log_{10}(R) (log_{10}(cm))')
ylabel('log_{10}(L) (log_{10}(cm))')
zlabel('Jsc')
name2b=sprintf('Radial cell Jsc with Ln=%s, Na=%s, Nd=%s, Sn=%s,maxEff=%s',
t2,t8,t9,t3, maxeff);
title(name2b)

figure(3)
surf(log10(R),log10(L),matrixVoc(2:(nL+1),2:(nR+1)))
xlabel('log_{10}(R) (log_{10}(cm))')
ylabel('log_{10}(L) (log_{10}(cm))')
zlabel('Voc')
name2c=sprintf('Radial cell Voc with Ln=%s, Na=%s, Nd=%s, Sn=%s,maxEff=%s',
t2,t8,t9,t3, maxeff);
title(name2c)

figure(4)
surf(log10(R),log10(L),matrixff(2:(nL+1),2:(nR+1)))
xlabel('log {10}(R) (log {10}(cm))')
ylabel('log_{10}(L) (log_{10}(cm))')
zlabel('ff')
name2d=sprintf('Radial cell ff with Ln=%s, Na=%s, Nd=%s, Sn=%s,maxEff=%s', t2,t8,t9,t3,
maxeff);
title(name2d)

beep
```

A.1.1 depletionregion.m

```
function
[x1,x2,x3,x4,Vbi]=depletionregion(Nd,Na,R,epsilonp,epsilonn,ni
,bias,windowwidth)
% depletionregion.m %calculates the thickness of each
%region of the pn junction in the cylindrical geometry, and
the built in
%voltage, given certain dopant densities and a wire of a given
radius and
%minimum emitter thickness, at a given bias
q=1.60219e-19;
kB=1.3807e-23;
T=300;
Vbi=kB*T/q*log(Na*Nd/ni^2);
if bias>=Vbi
    x1=0;
    x2=0;
    x3=0;
    x4=0;
    Vbi=0;
    %disp('3')
elseif bias<Vbi
    x3guess=sqrt(2*Nd*epsilonn*epsilonp*(Vbi-
bias)/(q*Na*(Nd*epsilonn+Na*epsilonp)));
    x3old=0;
    x3new=sqrt(2*Nd*epsilonn*epsilonp*(Vbi-
bias)/(q*Na*(Nd*epsilonn+Na*epsilonp)));
    %disp('4')

    while abs(x3old-x3new)>1e-9
        x3old=x3new;
        x3new=FZERO(@depletion,x3old,[],Vbi-
bias,0,epsilonp,epsilonn,Na,Nd);
    end
    x3max=x3new;
    x2max=sqrt(Na/Nd*x3max^2+x3max^2)-x3max;
    %VBI=q*Na/(4*epsilonp)*x3max^2+q*Nd/(4*epsilonn)*x3max^2-
q*Nd/(4*epsilonn)*R^2+q*Nd/(2*epsilonn)*R^2*log(R/x3max);
    if (x2max+x3max)>=R
        x4=0;
        x1=0;
        x2=x2max*R/(x2max+x3max);
        x3=x3max*R/(x2max+x3max);
        Vbi=(q*Na/(4*epsilonp)*x3^2-
q*Nd/(4*epsilonn)*((x3+x2)^2-
x3^2)+q*Nd/(2*epsilonn)*(x3+x2)^2*(log((x3+x2)/x3)));
```

```
        %disp('5')
    elseif (x2max+x3max)<R
        x4old=1;
        x4new=0;
        while abs(x4old-x4new)>1e-9
            x4old=x4new;
            x3=FZERO(@depletion,x3guess,[],Vbi-
bias,x4old,epsilonp,epsilonn,Na,Nd);
            x2=sqrt(Na*((x3+x4old)^2-x4old^2)/Nd+(x3+x4old)^2)-x3-
x4old;
            if x3>=(R-windowwidth)
                x1=R-x2-x3;
                x4new=0;
            elseif x3<(R-windowwidth)
                x1=max(0,windowwidth-x2);
                x4new=max(0,R-x1-x2-x3);
            end
        end
        x4=x4new;
    else
        disp('error 2')
    end
else
    disp('error 3')
end



end
```

A.1.2 depletion.m

```
function output=depletion(x3,V,x4,epsilonp,epsilonn,Na,Nd)
%% depletion.m
%is used to calculate the value of x3 that self-consistently
gives the
%correct voltage drop across the pn junction, in the
cylindrical geometry
q=1.60219e-19;
d2=x3+x4;
x2=sqrt(Na*(d2^2-x4^2)/Nd+d2^2)-d2;
if x4>0
    output=V-(q*Na/(4*epsilonp)*(d2^2-x4^2)-
q*Na/(2*epsilonp)*x4^2*log(d2/x4)-
```

```
q*Nd/(4*epsilonn)*((d2+x2)^2-
d2^2)+q*Nd/(2*epsilonn)*(d2+x2)^2*(log((d2+x2)/d2)));
elseif x4==0
    output=V-(q*Na/(4*epsilonp)*d2^2-
q*Nd/(4*epsilonn)*((d2+x2)^2-
d2^2)+q*Nd/(2*epsilonn)*(d2+x2)^2*(log((d2+x2)/d2)));
end



end
```

A.2 Simulation code for the nano Particle diameter

This is the simulation code for the nano particle diameter

```
t = 0.17;
n= [0.5,1,2,2.5];
h = 0:1:20;
for j=1:4
      A(j)= t^0.5*(82-151*n(j)+1200*n(j)^2-366*n(j)^3);
      B(j)= 1.05+0.523*n(j)-0.128*n(j)^2;
end

d1= A(1).*h.^2.*exp(-B(1).*h.^0.5)
d2= A(2).*h.^2.*exp(-B(2).*h.^0.5)
d3= A(3).*h.^2.*exp(-B(3).*h.^0.5)
d4= A(4).*h.^2.*exp(-B(4).*h.^0.5)
figure
plot(h,d1,'--r^',h,d2,'--go',h,d3,'--bs',h,d4,'--cd')
title('At constant TEOS 0.17M')
xlabel('Water concentration (M)')
ylabel('Average Diameter (nm)')
legend('0.5M NH3', '1.0M NH3', '2.0M NH3','2.5M NH3')
```

Bibliography

[1] E. S. Aydil, “Nanomaterials for Solar Cells,” *Nanotechnol. Law Bus.*, vol. 4, no. 3, p. 275, 2007.

[2] W. Shockley and H. J. Queisser, “Detailed balance limit of efficiency of p-n junction solar cells,” *J. Appl. Phys.*, vol. 32, no. 3, pp. 510–519, 1961.

[3] G. B. Haxel, J. B. Hedrick, and G. J. Orris, “Rare Earth Elements — Critical Resources for High Technology,” *United States Geol. Surv. Fact Sheet*, vol. 087, p. 4, 2002.

[4] S. Edition, *Photovoltaic Science Handbook of Photovoltaic Science*. 2011.

[5] C. B. Brabec, S. N.S., and J. C. Hummelen, “Plastic Solar Cells,” *Adv. Funct. Mater.*, vol. 11, no. 1, pp. 15–26, 2001.

[6] L. M. Chen, Z. Hong, G. Li, and Y. Yang, “Recent progress in polymer solar cells: Manipulation of polymer: Fullerene morphology and the formation of efficient inverted polymer solar cells,” *Adv. Mater.*, vol. 21, no. 14–15, pp. 1434–1449, 2009.

[7] B. Tian *et al.*, “Coaxial silicon nanowires as solar cells and nanoelectronic power sources,” *Nature*, vol. 449, no. 7164, pp. 885–889, 2007.

[8] O. Gunawan and S. Guha, “Characteristics of vapor-liquid-solid grown silicon nanowire solar cells,” *Sol. Energy Mater. Sol. Cells*, vol. 93, no. 8, pp. 1388–1393, 2009.

[9] C. Yung Kuo, C. Gau, and B. Tong Dai, “Photovoltaic characteristics of silicon nanowire arrays synthesized by vaporliquidsolid process,” *Sol. Energy Mater. Sol. Cells*, vol. 95, no. 1, pp. 154–157, 2011.

[10] W. F. Liu, J. I. Oh, and W. Z. Shen, “Light trapping in single coaxial nanowires for photovoltaic applications,” *IEEE Electron Device Lett.*, vol. 32, no. 1, pp. 45–47, 2011.

[11] V. Sivakov *et al.*, “Silicon Nanowire-Based Solar Cells on Glass : Synthesis , Optical Properties , and Cell Parameters 2009,” *Nano Lett.*, vol. 9, no. mc, pp. 1549–1554, 2009.

[12] T. Stelzner, M. Pietsch, G. Andr??, F. Falk, E. Ose, and S. Christiansen, “Silicon nanowire-based solar cells,” *Nanotechnology*, vol. 19, no. 29, 2008.

[13] E. Garnett and P. Yang, “Light trapping in silicon nanowire solar cells,” *Nano Lett.*, vol. 10, no. 3, pp. 1082–1087, 2010.

[14] S. M. Sze, *Semiconductor Devices: Physics and Technology*. 2006.

[15] K. Jager, O. Isabella, A. H. M. Smets, R. A. C. M. M. van Swaaij, and M. Zeman, “Solar Energy Fundamentals, Technology and Systems,” *Delf Univ. Technol.*, pp. 1–420, 2014.

[16] R. Foster, M. Ghassemi, and A. Cota, “Introduction to Solar Energy,” *Sol. Energy - Renew. Energy Environ.*, pp. 1–5, 2010.

[17] M. D. Kelzenberg *et al.*, “Single-nanowire Si solar cells,” *2008 33rd IEEE Photovolatic Spec. Conf.*, pp. 1–6, 2008.

[18] W. Lu and C. M. Lieber, “Semiconductor nanowires,” *J. Phys. D. Appl. Phys.*, vol. 39, no. 21, 2006.

[19] W. R. Wei *et al.*, “Above-11%-efficiency organic-inorganic hybrid solar cells with omnidirectional harvesting characteristics by employing hierarchical photon-trapping structures,” *Nano Lett.*, vol. 13, no. 8, pp. 3658–3663, 2013.

[20] U. Mehmood, S. Rahman, K. Harrabi, I. A. Hussein, and B. V. S. Reddy, “Recent Advances in Dye Sensitized Solar Cells,” *Adv. Mater. Sci. Eng.*, vol. 2014, pp. 1–12, 2014.

[21] S. Günes, H. Neugebauer, and N. S. Sariciftci, “Conjugated polymer-based organic solar cells,” *Chem. Rev.*, vol. 107, no. 4, pp. 1324–1338, 2007.

[22] J. Michallon, D. Bucci, A. Morand, M. Zanuccoli, V. Consonni, and A. Kaminski-

Cachopo, “Light trapping in ZnO nanowire arrays covered with an absorbing shell for solar cells,” *Opt. Express*, vol. 22, no. S4, p. A1174, 2014.

[23] R. Kapadia, Z. Fan, and A. Javey, “Design constraints and guidelines for CdS/CdTe nanopillar based photovoltaics,” *Appl. Phys. Lett.*, vol. 96, no. 10, pp. 1–4, 2010.

[24] W. J. Zhang, I. Bello, and S. T. Lee, “Vertically Aligned p-Type Single-Crystalline GaN Nanorod Arrays on n-Type Si for Heterojunction,” pp. 1–5, 2008.

[25] L. Yalçin and R. Öztürk, “Performance comparison of c-Si, mc-Si and a-Si thin film PV by PVsyst simulation,” *J. Optoelectron. Adv. Mater.*, vol. 15, no. 3–4, pp. 326–334, 2013.

[26] J. Kupec, R. L. Stoop, and B. Witzigmann, “Light absorption and emission in nanowire array solar cells,” *Opt. Express*, vol. 18, no. 26, p. 27589, 2010.

[27] B. M. Kayes, “Radial pn Junction, Wire Array Solar Cells,” *ProQuest Diss. Theses*, vol. 2009, p. 191, 2009.

[28] N. Technical, *NASA TECHNICAL HIGH EFFICIENCY SILICON*, no. December 1975. 2018.

[29] “ASTMG173.” .

[30] B. M. Kayes, H. A. Atwater, and N. S. Lewis, “Comparison of the device physics principles of planar and radial p-n junction nanorod solar cells,” *J. Appl. Phys.*, vol. 97, no. 11, 2005.

[31] S. Petrosyan, A. Yesayan, and S. Nersesyan, “Theory of Nanowire Radial pn-Junction,” *Int. J. …*, vol. 6, no. 11, pp. 1065–1070, 2012.

[32] W. Stober and A. Fink, “Controlled Growth of Monodispersed Silica Spheres in the Micron Size Range,” *J. Colloid Interface Sci.*, vol. 26, pp. 62–69, 1968.

[33] C. Engineering, “PREPARATION OF MONODISPERSE SILICA PARTICLES: C O N T R O L O F S I Z E AND M A S S FRACTION G.H. B O G U S H , M.A. T R A C Y and C.F. Z U K O S K I IV,” vol. 104, pp. 95–106, 1988.

[34] N. Van Minh, N. N. Son, N. Thi, H. Lien, and C. M. Hoang, “Non-close packaged monolayer of silica nanoparticles on silicon substrate using HF vapour etching,” vol. 12, pp. 656–659, 2017.

[35] Y. Wang, L. Chen, and H. Yang, “Large-area self assembled monolayers of silica microspheres formed by dip coating.,” *Mater. Sci.*, vol. 28, no. 2, pp. 467–478, 2010.

[36] H. Y. Ko, H. W. Lee, and J. Moon, “Fabrication of colloidal self-assembled monolayer (SAM) using monodisperse silica and its use as a lithographic mask,” *Thin Solid Films*, vol. 447–448, pp. 638–644, 2004.